# Effects of nanoparticle size on surface dynamics and thermal performance in film boiling of $Al_2O_3$ water-based nanofluids

Yahyaee, A.; Vatankhah, P.; Sørensen, H.

*Published in:*
Colloids and Surfaces A: Physicochemical and Engineering Aspects

*DOI (link to publication from Publisher):*
10.1016/j.colsurfa.2024.134267



*Publication date:*
2024

*Document Version*
Publisher's PDF, also known as Version of record

Colloids and Surfaces A: Physicochemical and Engineering Aspects 696 (2024) 134267

Contents lists available at ScienceDirect

Colloids and Surfaces A: Physicochemical and Engineering Aspects

journal homepage: www.elsevier.com/locate/colsurfa

# Effects of nanoparticle size on surface dynamics and thermal performance in film boiling of $Al_2O_3$ water-based nanofluids

A. Yahyaee [a,*], P. Vatankhah [b], H. Sørensen [a]

[a] AAU Energy, 9220 Aalborg East, Denmark
[b] School of Biomedical Engineering, Faculty of Engineering, The University of Sydney, Darlington, NSW 2008, Australia

## GRAPHICAL ABSTRACT

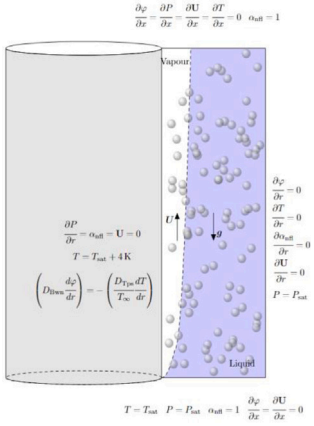


Study on the impact of Alumina nanoparticle size on film boiling in water-based nanofluids.

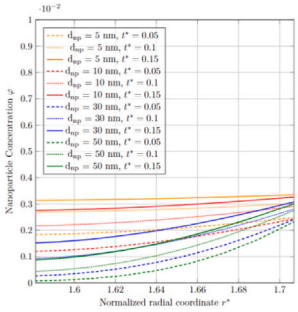


Smaller nanoparticles exhibit higher concentrations on the heated wall compared to larger nanoparticles.

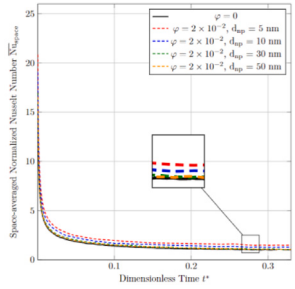


5 nm and 10 nm nanoparticles enhance thermal removal efficiency. 30 nm and 50 nm perform closely, indicating a size threshold.

## ARTICLE INFO

*Keywords:*
Nanofluid film boiling
Particle size
Surface deposition
Continuous-Species-Transfer method
Nanoparticle Brownian dynamics

## ABSTRACT

This study investigates the impact of nanoparticle diameter on film boiling in $Al_2O_3$ water-based nanofluids along a vertical cylinder, focusing on nanoparticle sizes of 5 nm, 10 nm, 30 nm, and 50 nm. Using a Continuous-Species-Transfer method within a Computational Multi-Fluid Dynamics framework, the behavior of nanoparticles in both liquid and vapor states is simulated, considering Brownian motion and thermophoretic effects. A 2D axisymmetric analysis reveals how nanoparticle sizes influence temperature gradients, nanoparticle concentration patterns, thermophysical properties, and the Nusselt number to assess heat transfer efficiency. Findings indicate that during film boiling, smaller nanoparticles exhibit higher concentrations on the heated

* Corresponding author.
*E-mail address:* ayahyaee@outlook.com (A. Yahyaee).

https://doi.org/10.1016/j.colsurfa.2024.134267
Received 20 February 2024; Received in revised form 27 April 2024; Accepted 13 May 2024
Available online 16 May 2024

Thermophoretic behavior

wall over time. Additionally, nanofluids with smaller particles demonstrate higher thermal conductivity and viscosity near the heated wall, along with lower surface tension. Interestingly, nanofluids with 30 nm and 50 nm nanoparticles perform closely, indicating a size threshold beyond which further reductions do not significantly enhance boiling heat transfer. In contrast, nanofluids containing 5 nm and 10 nm nanoparticles exhibit markedly superior thermal removal efficiency, underscoring the critical role of nanoparticle size in optimizing film boiling performance.

## 1. Introduction

In recent times, the study of nanofluid boiling processes has gained significant traction, highlighting its importance across various sectors such as propulsion systems in heavy vehicles, energy generation, advanced electronic cooling systems, and thermal management in aerospace. A particular focus within this domain is the efficient heat transfer in high heat flux systems, where two-phase flow plays a pivotal role. In such systems, the ability to effectively transfer heat to the coolant often becomes a design bottleneck. Utilizing two-phase flow can optimize this heat transfer, especially in the nucleate boiling regime, characterized by a high heat transfer coefficient. However, this process is constrained by the departure from nucleate boiling (DNB) or critical heat flux (CHF). Upon reaching CHF, the system transitions to film boiling, marked by the formation of a thin vapor layer that drastically reduces heat transfer capabilities, subsequently elevating the wall temperatures [1]. This transition, crucial in systems where overheating can lead to significant operational hazards, underpins the necessity to explore film boiling in greater depth.

Previous research has predominantly focused on pool [2–7] and flow boiling [8–11] of nanofluids. Nonetheless, the specific study of film boiling in nanofluids emerges as an essential yet less explored area. This is particularly relevant in industrial applications subjected to extreme thermal conditions, where a thorough comprehension of film boiling is indispensable [12–14]. The use of nanofluids as heat carriers, capable of operating at high heat fluxes introduces additional complexity, demanding a combination of computational [15–17] and experimental methods [18,19] for a comprehensive analysis.

Derived from the foundational theories of Maxwell [20], the enhancement of heat transfer properties through the addition of particles to base fluids such as water and oil is an established practice in the realm of thermal engineering [21,22]. The creation of nanofluids, involving the infusion of nanoparticles into these fluids, represents a notable advancement in this area [23]. These nanofluids, typically composed of particles less than 100 nm in size, are engineered to maximize thermal conductivity while minimizing the concentration of nanoparticles. The unique molecular dynamics of nanofluids enable evenly distributed nanoparticles to provide significant advantages, including enhanced heat transfer, efficient cooling in microchannels without blockages, and reductions in erosion, pumping power requirements, while improving the thermal conductivity and stability of the mixture. The diverse benefits of nanofluids have opened up new research area in nanotechnology, playing a pivotal role in advancing heat transfer and energy efficiency across various sectors such as transportation cooling systems, power generation, space industries, microelectronics, and biomedical devices [24].

The impact of nanoparticles on the thermophysical characteristics and surface dynamics during nanofluid boiling processes has received significant attention [25–28]. In high-temperature scenarios, nanoparticles not only modify the surface characteristics but also interact dynamically with the fluid's thermal properties [29,30]. The deposition of nanoparticles on surfaces modifies crucial parameters such as surface wettability, heat transfer coefficients, and capillary action [31–33]. This formation of a nanoparticle layer acts as an interfacial coating, thereby substantially increasing the efficiency of heat transfer processes [34].

Moreover, nanoparticles significantly impact the wettability of surfaces, a critical aspect that directly affects the dynamics of boiling. Wettability, in this context, refers to the capacity of a liquid to maintain contact with a solid surface, even in the presence of vapor. This property influences essential boiling parameters such as the radius of the triple line (where liquid, gas, and solid phases meet) and the contact angle, which are determined by the complex interplay of forces among the liquid, gas, and solid phases at the three-phase interface [35,36]. The type and concentration of nanoparticles can markedly alter surface tension and contact angles. For instance, nanofluids containing silica nanoparticles have demonstrated lower surface tension compared to pure water, affecting crucial boiling features like bubble size and the dynamics of their detachment from the surface [27,37,38].

Advancements in CFD research concerning nanofluid boiling have progressed remarkably, evolving from initial studies concentrated on enhancing heat transfer to more complex analyses that include the dynamics of nanoparticles. Significant contributions to this field encompass Abedini et al.'s investigation into subcooled flow boiling of $Al_2O_3$-Water nanofluid [39], Shoghl et al.'s exploration of bubble dynamics in pool boiling with CuO and $Al_2O_3$ water-based nanofluids [40], and Qi et al.'s research on the impact of $TiO_2$ nanoparticles within water-based nanofluids [41]. Additionally, Abdollahi et al. delved into how various nanoparticle types and concentrations influence boiling in laminar micro-channel flows [42], whereas Mohammed et al. demonstrated that the vapor produced during boiling intensifies with particle loading and temperature, and diminishes with increased fluid velocity [43].

Recent developments include Li et al.'s investigation into the effects of gravity on boiling fluids [44]. Zaboli et al. explored the influence of varying nanoparticle concentrations on the pool boiling characteristics of nanofluids [45]. Additionally, Bahiraei et al. contributed insights into the entropy generation and exergy efficiency in the flow of Ag-water nanofluids [46].

Delving further into the subject, CFD studies on nanofluid boiling have evolved significantly, taking inspiration from the work of Buongiorno [47]. This study introduced Brownian motion and thermophoresis as key mechanisms driving nanoparticle movement. This line of inquiry has been further developed by a wide array of researchers [48–54]. Among these, Yang et al. [48] explored the convective heat transfer of nanofluids within a concentric annulus. Similarly, Malvandi et al. [49] investigated mixed convective heat transfer of nanofluids through a concentric vertical annulus, and another study by Malvandi et al. [50] examined how nanoparticle migration influences heat transfer enhancement during film boiling of nanofluids over a vertical cylinder. Hedayati et al. conducted research on the effects of nanoparticle migration and asymmetric heating on mixed convection of $TiO_2$–Water nanofluid inside a vertical microchannel [51] and a horizontal microchannel [52]. Malvandi [53] has explored the dynamics of magnetic nanofluids during boiling. Another notable contribution comes from Wang et al. [54], who conducted a numerical study focusing on the deposition of nanoparticles in microchannel cooling systems, emphasizing the critical role of nanoparticle motion in nanofluid thermal management strategies. These collective efforts mark a significant evolution in the field, effectively linking foundational research to more advanced studies that consider the intricate movement of nanoparticles.

In the most recent advancements in CFD simulations of nanofluid boiling, Yahyaee et al. [29] developed a novel approach to CFD simulation that includes the migration of nanoparticles between phases using the continuous-species-transfer (CST) method. Following this development, Yahyaee [30] investigated the influence of nanoparticle shape on the boiling of nanofluids. This study demonstrated that nanofluids

## Nomenclature

### Acronyms

| | |
|---|---|
| CMFD | Computational Multi-Fluid Dynamics framework for simulating interactions between multiple fluid phases. |
| CHTC | Convective heat transfer coefficient. |
| CSF | Continuum Surface Force model, used for simulating surface tension effects in fluids. |
| CST | Continuous-Species-Transfer model, employed for modeling species exchange between phases. |
| VOF | Volume of Fluid method, a technique for tracking fluid interfaces. |

### English symbols

| | |
|---|---|
| $\dot{m}$ | Mass transfer rate between phases. |
| **f** | Force vector in a physical system. |
| **g** | Vector representing gravitational acceleration. |
| **U** | Velocity vector of fluid flow. |
| $H_{\mathrm{cnst}}$ | Henry's law constant, defining solubility. |
| $L_{\mathrm{fv}}$ | Latent heat of vaporization of a fluid. |
| $\phi$ | Nanoparticle concentration in vapor or liquid. |
| $\varphi$ | Total nanoparticle concentration in the system. |
| C | Isothermal compressibility coefficient. |
| c | Specific heat at constant pressure. |
| D | Coefficient of diffusivity or diffusion. |
| d | Characteristic dimension, typically diameter. |
| h | Enthalpy associated with phase change. |
| k | A constant, often in proportionality relations. |
| M | Molar mass of a substance. |
| Nu | Nusselt number, representing convective heat transfer efficiency. |
| p | Pressure within the fluid. |
| R | Universal gas constant, applicable in ideal gas calculations. |
| T | Temperature, indicating thermal state. |
| t | Time variable in temporal analyses. |

### Greek symbols

| | |
|---|---|
| $\alpha$ | Volume fraction of a phase in a mixture. |
| $\delta$ | Characteristic thickness of a layer or boundary. |
| $\gamma$ | Evaporation rate coefficient. |
| $\kappa$ | Curvature measure at an interface. |
| $\mu$ | Dynamic viscosity, quantifying fluid resistance to deformation. |
| $\rho$ | Density, indicative of mass per unit volume. |
| $\sigma$ | Surface tension coefficient in fluid mechanics. |
| $\boldsymbol{\tau}$ | Viscous stress tensor in fluids. |
| $k$ | Thermal conductivity coefficient. |

### Subscripts

| | |
|---|---|
| $\alpha$ | Volume fraction of a specific phase. |
| $\delta$ | Represents thin films or layers. |
| $\infty$ | Condition at an infinitely far distance. |
| ana | Indicates analytical results. |
| bf | Indicates the base fluid in a mixture. |
| Bltzmn | Related to the Boltzmann constant in thermodynamics. |
| Bwn | Associated with Brownian motion phenomena. |
| c | Related to compressive properties. |
| f | Referring to a facet or face in computational domains. |
| grav | Pertains to gravitational effects. |
| k | Index for computational nodes. |
| l | Referring to the liquid phase in a system. |
| nfl | Denotes the liquid phase with nanoparticles. |
| nfv | Refers to the vapor phase containing nanoparticles. |
| np | Refers to nanoparticles. |
| num | Denotes numerical results. |
| Nu | Nusselt number, important in heat transfer studies. |
| p | Indicative of a constant pressure condition. |
| r | Relates to a reference or baseline state. |
| sat | Indicates saturation conditions in thermodynamics. |
| Tps | Linked to Thermophoresis processes. |
| $\sigma$ | Refers to surface phenomena or interfacial properties. |
| T | Temperature in a thermal context. |

### Superscripts

| | |
|---|---|
| ,, | Indicates a surface transfer rate. |
| ,,, | Denotes a volumetric transfer rate. |
| * | Signifies a dimensionless quantity. |

containing blade-shaped nanoparticles exhibit superior heat transfer capabilities compared to those with other shapes such as spheres, bricks, cylinders, and platelets.

The significance of nanoparticle size in nanofluid boiling has been a prominent research topic in recent years. This part of the literature review synthesizes results from various studies to provide a chronological examination of how nanoparticle size impacts the characteristics of nanofluid boiling. The investigation into the effects of nanoparticle size on nanofluid boiling characteristics has been a central focus. Peng et al. [55] performed a crucial study on the nucleate pool boiling heat transfer in a refrigerant/oil mixture with Cu nanoparticles of 20, 50, and 80 nm. Their findings demonstrated that decreasing the nanoparticle size from 80 nm to 20 nm could enhance the boiling heat transfer coefficient by up to 23.8%. Another significant contribution was made by Souza et al. [56], who examined the effects of 10 nm and 80 nm maghemite nanoparticles on the nucleate boiling of HFE7100. They observed a 55% increase in the heat transfer coefficient with the smaller nanoparticles, while the larger nanoparticles resulted in a reduction of approximately 29%.

Hu et al. [57] contributed significantly to the understanding of $SiO_2$-EG/sDW nanofluids. Their research revealed that reducing the nanoparticle diameter from 120 nm to 84 nm resulted in an increase in the

boiling heat transfer coefficient, with the most notable improvement observed at a concentration of 0.25 vol%. Simultaneously, Sayahi and Bahrami [58] examined various nanoparticles in water-based nanofluids and found that $\gamma$-alumina significantly enhanced the pool boiling heat transfer coefficient. In contrast, larger silica nanoparticles were less effective at reducing the heat transfer coefficient compared to their smaller counterparts.

Liu et al. [59], utilizing the Wilson Plot method, studied the convective heat transfer coefficient (CHTC) of $SiO_2$, $TiO_2$, and $Al_2O_3$ nanoparticles in water. They concluded that the addition of nanoparticles generally increased the CHTC, with $Al_2O_3$ nanoparticles at a 0.5 vol% concentration achieving a notable 45% increase. Moreover, simply reducing nanoparticle size and increasing the nanofluid flow rate does not necessarily lead to CHTC enhancement; rather, these changes can have adverse effects. It is concluded that the enhancement depends on the stability of the dispersed nanoparticles, which can be characterized by their overall mean size and zeta potential as useful measures.

### Inspirations and contributions

The critical review of existing literature underscores several research gaps, prompting the focus of the present study:

- The existing body of CFD and experimental research has not comprehensively addressed the effects of nanoparticle sizes, especially in the context of film boiling.
- Despite significant advancements in understanding the forces affecting nanoparticles, such as Brownian diffusion and thermophoresis, as outlined by Buongiorno [47], there remains a notable gap in CFD research [39–46]. This gap concerns the explicit incorporation of dedicated nanoparticle transport equations. While some CFD studies have integrated these equations [48–52], their primary focus has often been on the insulating role of the vapor layer in film boiling, thus neglecting the dynamic interactions between the nanofluid's liquid phase and the vapor layer. This study utilizes the CFD method introduced by Yahyaee et al. [29], where the CFD simulation considers both the vapor and liquid layers as well as the deposition of nanoparticles.

Given the existing research gaps, this study focuses on the effect of nanoparticle sizes, performing a detailed CFD analysis of film boiling in alumina ($Al_2O_3$) water-based nanofluids. We examine nanoparticle sizes ranging from 5 nm to 50 nm, each impacting the fluid dynamics and heat transfer properties differently.

The CFD model used in this study, based on the work by Yahyaee et al. [29], employs the CST methodology in Computational Multi-Fluid Dynamics (CMFD). This method models key behaviors, such as nanoparticle concentration on the heated wall and their movement between vapor and liquid phases. This approach is crucial for capturing the intricate dynamics at the vapor–liquid interface, often missed in conventional film boiling research. By incorporating considerations like Brownian motion and thermophoresis, this method seeks to expand on the insights provided by the CST methodology. A 2D axisymmetric analysis around a cylindrical surface is conducted to study the distinct role of nanoparticle sizes in influencing film boiling dynamics. It particularly explores how different sizes affect essential factors like nanoparticle concentration on the heated surface, temperature variations, and the overall thermophysical properties of the nanofluid. Additionally, the Nusselt number is also assessed as a critical measure of heat transfer efficiency in film boiling scenarios. This analysis is vital for elucidating the potential heat transfer improvements with different nanoparticle sizes, thus offering new perspectives on optimizing nanofluid formulations for better thermal performance in industrial settings.

## 2. Mathematical modeling approach

### 2.1. Formulation of governing equations

In this study, the Volume of Fluid (VOF) method is used to model the complex behavior of a two-phase system, with a particular focus on the changes between phases and the thermal properties within nanofluids. The VOF method is a powerful computational tool that accurately tracks and models the boundary between two non-mixing fluid phases, such as liquid and vapor in nanofluids.

The model's equations are developed from volume-averaged conservation laws that are applied conditionally, allowing for a detailed representation of the behavior of each phase:

*Mass Conservation*: The mass conservation principle is integral to understanding the fluid dynamics within the system. It is described by the following equation [60]:

$$\frac{\partial \rho}{\partial t} + \nabla \cdot (\rho \mathbf{U}) = 0, \tag{1}$$

where $\rho$ represents the fluid density and $\mathbf{U}$ denotes the velocity field. This equation ensures that the mass within a control volume remains constant over time, accounting for the inflow and outflow of mass.

*Momentum Conservation*: The momentum conservation equation takes into account the forces acting on the fluid elements, including pressure, viscous, gravitational, and surface tension forces [60,61]:

$$\frac{\partial (\rho \mathbf{U})}{\partial t} + \nabla \cdot (\rho \mathbf{U}\mathbf{U}) = -\nabla p + \nabla \cdot \boldsymbol{\tau} + \mathbf{f}_{\text{grav}} + \mathbf{f}_{\sigma}. \tag{2}$$

In this equation, $p$ represents pressure, $\boldsymbol{\tau}$ denotes the stress tensor, $\mathbf{f}_{\text{grav}}$ is the gravitational force, and $\mathbf{f}_{\sigma}$ signifies surface tension forces.

Surface tension effects are critical in the dynamics of multiphase flows, especially at the interface. The Continuous-Surface-Force (CSF) model [62] is utilized to model these forces effectively:

$$\mathbf{f}_{\sigma} = \sigma \kappa \nabla \alpha_{\text{nfl}}, \quad \text{where} \quad \kappa = -\nabla \cdot \left( \frac{\nabla \alpha_{\text{nfl}}}{|\nabla \alpha_{\text{nfl}}|} \right), \tag{3}$$

where $\sigma$ is the surface tension coefficient, $\kappa$ is the curvature of the interface, and $\alpha_{\text{nfl}}$ is the volume fraction of the liquid nanofluid phase.

*Phase Fraction Evolution*: The evolution of the liquid nanofluid's phase fraction within the computational domain is modeled as follows [63,64]:

$$\frac{\partial \alpha_{\text{nfl}}}{\partial t} + \nabla \cdot (\mathbf{U} \alpha_{\text{nfl}}) + \nabla \cdot (\mathbf{U}_{\text{r}} \alpha_{\text{nfl}} (1 - \alpha_{\text{nfl}})) = -\dot{m}''' \left[ \frac{1}{\rho_{\text{nfl}}} - \alpha_{\text{nfl}} \left( \frac{1}{\rho_{\text{nfl}}} - \frac{1}{\rho_{\text{nfv}}} \right) \right], \tag{4}$$

To maintain a sharp interface and minimize numerical diffusion, the relative velocity $\mathbf{U}_r$ at the interface is modeled using a compressive velocity $\mathbf{U}_c$ approach as it is introduced by Weller and Olsson [65,66]:

$$\mathbf{U}_c = \min \left[ c_\alpha |\mathbf{U}|, \max(|\mathbf{U}|) \right] \frac{\nabla \alpha_{\text{nfl}}}{|\nabla \alpha_{\text{nfl}}|}, \tag{5}$$

where $c_\alpha$ is a coefficient typically chosen between 1 and 4 to effectively manage the interface sharpness.

*Governing Equation for Nanoparticle Transport Dynamics:* This study adopts the methodology introduced by Yahyaee et al. [29] to investigate nanoparticle behavior in film boiling scenarios. Yahyaee et al. formulated their approach around a fundamental governing equation widely acknowledged in prominent fluid dynamics research [47–52]:

$$\frac{\partial \phi}{\partial t} + \nabla \cdot (\phi \mathbf{U}) = \nabla \cdot (D_{\text{Bwn}} \nabla \phi) + \nabla \cdot \left[ D_{\text{Tps}} \frac{\nabla T}{T_\infty} \right]. \tag{6}$$

Eq. (6), traditionally applied in single-phase studies. In the approach by Yahyaee et al. the analysis extends to effectively observe nanoparticle behavior across both the vapor and liquid phases of nanofluids, with a focus on their interactions at the interface. By incorporating the CST method [67], as detailed in the studies by Yahyaee et al. [29], a more encompassing governing equation is formulated. This

equation is designed to capture the varied transport phenomena at the nanofluid interface, thus enhancing the understanding of how nanoparticles behave differently in each phase [29,30]:

$$\frac{\partial \varphi}{\partial t} + \nabla \cdot (\varphi \mathbf{U}) = \nabla \cdot \left(D'_{\mathrm{Bwn}} T \nabla \varphi\right) + \nabla \cdot \left(\varphi T \nabla D'_{\mathrm{Bwn}}\right) + \nabla \cdot \left(\varphi D'_{\mathrm{Bwn}} \nabla T\right) - \nabla \cdot \left[\left(\frac{\overline{D'_{\mathrm{Bwn}}}^{\mathrm{nfl}} - \overline{D'_{\mathrm{Bwn}}}^{\mathrm{nfv}}/\mathrm{H_{cnst}}}{\alpha_{\mathrm{nfl}} + (1-\alpha_{\mathrm{nfl}})/\mathrm{H_{cnst}}}\right) \varphi T \nabla \alpha_{\mathrm{nfl}}\right] - \nabla \cdot \left[\left(\frac{\alpha_{\mathrm{nfl}} \overline{D'_{\mathrm{Bwn}}}^{\mathrm{nfl}} + (1-\alpha_{\mathrm{nfl}}) \overline{D'_{\mathrm{Bwn}}}^{\mathrm{nfv}}/\mathrm{H_{cnst}}}{\alpha_{\mathrm{nfl}} + (1-\alpha_{\mathrm{nfl}})/\mathrm{H_{cnst}}}\right) \varphi \nabla T\right] + \nabla \cdot \left[\left(\frac{\alpha_{\mathrm{nfl}} \overline{D'_{\mathrm{Tps}}}^{\mathrm{nfl}} + (1-\alpha_{\mathrm{nfl}}) \overline{D'_{\mathrm{Tps}}}^{\mathrm{nfv}}/\mathrm{H_{cnst}}}{\alpha_{\mathrm{nfl}} + (1-\alpha_{\mathrm{nfl}})/\mathrm{H_{cnst}}}\right) \varphi \nabla T\right]. \quad (7)$$

where the coefficients $D'_{\mathrm{Bwn}}$ and $D'_{\mathrm{Tps}}$ are:

$$D'_{\mathrm{Bwn}} = D_{\mathrm{Bwn}}/T, \quad D'_{\mathrm{Tps}} = D_{\mathrm{Tps}}/(T_\infty \varphi). \quad (8)$$

The coefficients $D_{\mathrm{Bwn}}$ and $D_{\mathrm{Tps}}$ denote the diffusion factors for Brownian motion and thermophoresis respectively and are mathematically defined as:

$$D_{\mathrm{Bwn}} = \frac{k_{\mathrm{Bltzmn}} T}{3\pi \mu_{\mathrm{bf}} d_{\mathrm{np}}}, \quad (9)$$

$$D_{\mathrm{Tps}} = \beta \frac{\mu_{\mathrm{bf}}}{\rho_{\mathrm{bf}}} \varphi, \quad (10)$$

where $\beta$ equals $0.26 k_{\mathrm{bf}}/(2k_{\mathrm{bf}} + k_{\mathrm{np}})$.

Eq. (7) is meticulously designed to address the entire computational domain, focusing on the transport of nanoparticles and capturing the intricate dynamics at the fluid interface. This equation's adaptability ensures that the complexities of nanoparticle movement, particularly in the context of phase change and interfacial tension, are modeled. The detailed representation of nanoparticle behavior provided by this approach is critical for a thorough understanding and optimization of the film boiling process in nanofluid systems.

*Energy Conservation Equation to Integrate Nanoparticle Dynamics:* The fundamental energy conservation equation is adapted to include the effects of nanoparticles within the boiling dynamics of nanofluids [60]:

$$\frac{\partial(\rho c_{\mathrm{p}} T)}{\partial t} + \nabla \cdot (\rho c_{\mathrm{p}} \mathbf{U} T) = \nabla \cdot (k \nabla T) - \dot{m}''' L_{\mathrm{fv}}, \quad (11)$$

Following studies such as Malvandi et al. [50] on nanofluids, the equation also incorporates the effects of Brownian motion and thermophoresis:

$$+\rho_{\mathrm{np}} c_{\mathrm{p,np}} \left[D_{\mathrm{Bwn}} \nabla \phi \cdot \nabla T + \frac{D_{\mathrm{Tps}}}{T_\infty} \nabla T \cdot \nabla T\right], \quad (12)$$

Originally designed for single-phase analysis, Eq. (12) has been expanded to encompass multi-phase scenarios, capturing the interactions among vapor, liquid, and their interfaces. Following the advancements by Yahyaee et al. [29], the revised thermal energy conservation equation now comprehensively addresses all phases and the intricate dynamics of nanoparticle movement [29,30]:

$$\frac{\partial(\rho c_{\mathrm{p}} T)}{\partial t} + \nabla \cdot (\rho c_{\mathrm{p}} \mathbf{U} T) = \nabla \cdot (k \nabla T) - \dot{m}''' L_{\mathrm{fv}} + \rho_{\mathrm{np}} c_{\mathrm{p,np}} \left(\frac{\alpha_{\mathrm{nfl}} \overline{D'_{\mathrm{Bwn}}}^{\mathrm{nfl}} + (1-\alpha_{\mathrm{nfl}}) \overline{D'_{\mathrm{Bwn}}}^{\mathrm{nfv}}/H_{\mathrm{cnst}}}{\alpha_{\mathrm{nfl}} + (1-\alpha_{\mathrm{nfl}})/H_{\mathrm{cnst}}}\right) T \nabla \varphi \nabla T + \rho_{\mathrm{np}} c_{\mathrm{p,np}} \left(\frac{\alpha_{\mathrm{nfl}} \overline{D'_{\mathrm{Tps}}}^{\mathrm{nfl}} + (1-\alpha_{\mathrm{nfl}}) \overline{D'_{\mathrm{Tps}}}^{\mathrm{nfv}}/H_{\mathrm{cnst}}}{\alpha_{\mathrm{nfl}} + (1-\alpha_{\mathrm{nfl}})/H_{\mathrm{cnst}}}\right) \varphi \nabla T \nabla T. \quad (13)$$

The phase change process and mass flux rate $\dot{m}'''$ are modeled using OpenFOAM, a well-known open-source CFD tool [65]. The interfaceHeatResistance model from OpenFOAM v2006, influenced by the research of Hardt and Wondra [68], plays a crucial role in this analysis. Additional details on the model and its implementation are available in the work by Hardt and Wondra [68] and the extensive OpenFOAM documentation.

### 2.2. Nanoparticles size and thermophysical property evaluation of nanofluids

Critical thermophysical properties such as density, specific heat capacity, viscosity, thermal conductivity, and surface tension are essential for analyzing multiphase flow and heat transfer in thermal systems. Accurately determining these properties is crucial for boiling simulations that involve nanofluids. In CFD simulations, these properties are derived using various correlations. The extensive literature [39–52] supports this approach. OpenFOAM, being open-source, allows for defining these properties through correlations that account for composition, size, and concentration. The mixture model, typically applied to fluid–solid mixtures, facilitates the calculation of density and specific heat capacity in nanofluids, as illustrated by the following equations [69]:

$$\rho_{\mathrm{nf\,lv}} = \varphi \rho_{\mathrm{np}} + (1-\varphi) \rho_{\mathrm{bf\,lv}}, \quad (14)$$

$$c_{\mathrm{p,nf\,lv}} = \frac{\varphi \rho_{\mathrm{np}} c_{\mathrm{p,np}} + (1-\varphi) \rho_{\mathrm{bf\,lv}} c_{\mathrm{p,bf\,lv}}}{\rho_{\mathrm{nf\,lv}}}, \quad (15)$$

where the subscripts np, bf lv, and nf lv refer to nanoparticles, liquid and vapor base fluid, and liquid and vapor nanofluid properties, respectively.

The correlation chosen for this analysis includes nanoparticle size to calculate the thermal conductivity, viscosity, and surface tension of nanofluids. This approach supports the study's goal to examine the effect of nanoparticle size on film boiling behavior in nanofluids. By incorporating nanoparticle size into these correlations, the analysis becomes more relevant and precise, enhancing the understanding of how size variations affect the thermal and flow properties of nanofluids during film boiling processes.

The widely recognized empirical correlation, proposed by Corcione [70] and based on extensive experimental data, is frequently used in numerous studies such as Heyhat et al. [71] and Wakif et al. [72]. This correlation allows for the prediction of the dynamic viscosity of nanofluids and is employed to calculate the viscosity in this study:

$$\frac{\mu_{\mathrm{nf\,lv}}}{\mu_{\mathrm{bf\,lv}}} = \frac{1}{1 - 34.87 \left(\frac{d_{\mathrm{np}}}{d_{\mathrm{f}}}\right)^{-0.3} \varphi^{1.03}}, \quad (16)$$

where $d_{\mathrm{f}}$ signifies the equivalent diameter of a base fluid molecule which is determined as follows:

$$d_{\mathrm{f}} = 0.1 \left(\frac{6\mathrm{M}}{\mathrm{N}\pi\rho_{\mathrm{f0}}}\right)^{1/3}, \quad (17)$$

where $d_{\mathrm{np}}$ is the diameter of the nanoparticles, M denotes the molecular weight of the base fluid, $N$ is Avogadro's number, and $\rho_{\mathrm{f0}}$ is the mass density of the base fluid at $T = 293$ K.

Based on Maxwell's well-known work, the effective thermal conductivity of a homogeneous suspension can be predicted as [20]:

$$\frac{k_{\mathrm{nf\,lv}}}{k_{\mathrm{bf\,lv}}} = \frac{k_{\mathrm{np}} + 2k_{\mathrm{bflv}} + 2(k_{\mathrm{np}} - k_{\mathrm{bflv}})\varphi}{k_{\mathrm{np}} + 2k_{\mathrm{bflv}} - (k_{\mathrm{np}} - k_{\mathrm{bflv}})\varphi} \quad (18)$$

Yu and Choi [73], in a widely recognized study, extended the Maxwell correlation (Eq. (18)) to include nanoparticle size for calculating the thermal conductivity of nanofluids. The modified correlation, now known as the Yu and Choi model, has gained prominence and is frequently employed in numerous studies. This model is utilized to calculate the thermal conductivity in the current study, as well as in the research conducted by Khalili Najafabadi [74] and Zhu [75]:

$$\frac{k_{\mathrm{nf\,lv}}}{k_{\mathrm{bf\,lv}}} = \frac{k_{\mathrm{np}} + 2k_{\mathrm{bflv}} + 2(k_{\mathrm{np}} - k_{\mathrm{bflv}})(1+\beta)^3\varphi}{k_{\mathrm{np}} + 2k_{\mathrm{bflv}} - (k_{\mathrm{np}} - k_{\mathrm{bflv}})(1+\beta)^3\varphi} \quad (19)$$

**Table 1**
Thermophysical properties of saturated water for the simulation of 2D film boiling and 2D axisymmetric vertical film boiling scenarios [79].

| | Dimension | Base fluid (Water) | Vapor phase |
|---|---|---|---|
| Thermal conductivity, $k$ | $W\,m^{-1}\,K^{-1}$ | 0.545 | 0.054 |
| Density, $\rho$ | $kg\,m^{-3}$ | 402.4 | 242.7 |
| Viscosity, $\mu$ | Pa s | $4.53\times10^{-5}$ | $3.23\times10^{-5}$ |
| Specific heat capacity $c_p$ | $J\,kg^{-1}\,K^{-1}$ | $2.18\times10^{5}$ | $3.52\times10^{5}$ |
| Latent heat, $h$ | $J\,kg^{-1}$ | $1.96\times10^{6}$ | $2.24\times10^{6}$ |
| Surface tension, $\sigma$ | $N\,m^{-1}$ | $7\times10^{-5}$ | – |

where $\beta$ is a factor considering the nanoparticle diameter, with $\beta = \frac{2h}{d_{np}}$, and $h$ is the radius of the microlayer around the spherical nanoparticle.

The study by Chinnam et al. [76] is known for presenting a comprehensive model that evaluates the effects of volume fraction, temperature, and nanoparticle size on the surface tension of nanofluids. This model, used to calculate the surface tension in this study, is encapsulated in the following equation:

$$\frac{\sigma_{nflv}}{\sigma_{bflv}} = a\varphi + b\left(\frac{T_0}{T}\right) + c\left(\frac{d_{np}}{d_f}\right) + D, \tag{20}$$

where $a = -1.02219$, $b = -0.27706$, $c = 0.00063558$, and $D = 1.17344$. Here, $\sigma_{nf}$ and $\sigma_{bf}$ represent the surface tensions of the nanofluid and base fluid, $\varphi$ denotes the nanoparticle volume fraction, and $d_{np}$ and $d_{bf}$ signify the nanoparticle and molecular diameters, respectively.

### 2.3. Computational problem configuration and setup

The main focus of this study is the thermal interaction of a vertical cylinder immersed in a nanofluid with a nanoparticle concentration of $\varphi = 1\times10^{-2}$ in the liquid phase, illustrated in Fig. 1. The investigation starts when the cylinder's surface temperature, $T_s$, exceeds the boiling point of the nanofluid, $T_{sat}$. This scenario prompts the formation of a vapor layer that encircles the cylinder and extends vertically along its length. The ascent of this vapor layer is primarily driven by buoyancy, with gravity playing a significant role in its movement. Although phenomena such as changes in the triple-line motion due to nanoparticle deposition are observed in nanofluid boiling, this study specifically examines film boiling in a water-$Al_2O_3$ nanofluid adjacent to a vertical cylinder. In this film boiling setup, an insulating vapor film helps minimize these effects by preventing direct contact between the liquid and the surface.

To improve computational efficiency, the initially three-dimensional (3D) problem is simplified to a two-dimensional (2D) axisymmetric model. The computational domain is modeled as a wedge, with the $z$-axis at the cylinder's vertical center serving as the axis of symmetry. This axisymmetric method is crucial for effectively simulating the relevant physical phenomena while using computational resources efficiently. In the OpenFOAM framework, the front and back boundaries of the domain are set as 'wedge' types, which is essential for simulating axisymmetric behaviors.

The simulation setup begins with an initial thin vapor film in direct contact with the cylinder surface. The boundary conditions, shown in Fig. 1, include a specific concentration boundary for nanoparticles on the cylinder surface. The dynamics of thermophoretic ($D_{Tps}$) and Brownian diffusion ($D_{Bwn}$) in the boundary condition are described by Eqs. (9) and (10). An important aspect of the boundary condition at the cylinder surface is the nanoparticle impermeability, ensuring no nanoparticle flux across the cylinder wall. This condition, often referred to as Stefan flow, is influenced by both concentration and temperature gradients. This boundary mechanism is grounded in the studies by Avramenko et al. [50,77,78].

The thermophysical properties of the base fluid, its vapor phase, and the $Al_2O_3$ nanoparticles utilized in this research are detailed in Tables 1 and 2.

**Table 2**
Properties of $Al_2O_3$ nanoparticles as used in the simulations.

| Property | Dimension | Value for $Al_2O_3$ |
|---|---|---|
| Thermal conductivity, $k$ | $W\,m^{-2}\,K^{-1}$ | 40 |
| Density, $\rho$ | $kg\,m^{-3}$ | 3970 |
| Specific heat capacity, $c_p$ | $J\,kg^{-1}\,K^{-1}$ | 765 |

### 2.4. Verification against Taylor's two-dimensional film boiling model

The computational solver's precision was assessed against Taylor's two-dimensional film boiling model for pure fluids, corroborated by experimental results. While the main focus of this research is on vertical film boiling, Taylor's model, typically used for horizontal film boiling, serves as a rigorous validation benchmark. The choice of Taylor's model is due to its accuracy and the availability of experimental data for comparison. This model is relevant to the vertical film boiling scenarios explored in this research. Essential thermophysical properties used in this validation phase are listed in Table 1. Simulations assumed no nanoparticles, and the setup's details, including boundary conditions and computational domain geometry, are shown in Fig. 2, with comprehensive descriptions found in previous studies [79–81].

The calculation of the Nusselt number in this 2D film boiling case aligns with the methodology by Esmaeeli and Tryggvason [82]:

$$\mathrm{Nu} = \frac{\int_0^L \left(\frac{L_{chrst}}{\Delta T}\left.\frac{\partial T}{\partial y}\right|_{y=0}\right) dx}{L}, \tag{21}$$

The characteristic length, $L_{chrst}$, is defined as:

$$L_{chrst} = \sqrt{\frac{\sigma}{(\rho_l - \rho_v)g}}. \tag{22}$$

The obtained Nusselt number is compared with Berenson's empirical results for two-dimensional film boiling [83]:

$$\mathrm{Nu} = 0.425\left[\frac{\rho_v(\rho_l - \rho_v)g(h_v - h_l)}{k_v\mu_v\Delta T}\right]. \tag{23}$$

Fig. 3 displays the simulation results, indicating an average Nusselt number of 4.6 on the cylinder's surface. This value closely aligns with the 4.25 Nusselt number from Berenson's formula, showing a minor discrepancy of 7.6%. This comparison substantiates the solver's ability to accurately simulate film boiling phenomena, mirroring the results from Berenson's empirical research.

### 2.5. Grid density and temporal resolution verification

To ensure the solution's accuracy, a grid density independence study was performed. This evaluation aimed to accurately delineate the vapor–liquid interface at a specific temporal snapshot, examining a range of grid configurations denoted by $N_{meshes} = [50\times50, 100\times100, 200\times200, 300\times300, 400\times400]$. Utilizing OpenFOAM's simpleGrading approach, with a grading ratio of $(15, 1, 1)$, facilitated a denser mesh near the heating surface essential for detailed vapor interface resolution. Fig. 4 showcases the precision in capturing the vapor interface across these mesh sizes.

After evaluating both the computational load and the accuracy of the results, a mesh configuration of $300\times300$ was selected for all future simulations. This mesh density provides a balance, offering near-equivalent accuracy to the $400\times400$ configuration but with a more efficient use of computational resources.

Subsequent to establishing mesh density, the study proceeded with analyzing the independence of time step size based on the Courant number. The selection of an appropriate time step is crucial in computational simulations to adhere to the Courant–Friedrichs–Lewy (CFL) condition, which serves as a guideline for numerical scheme stability. The CFL criterion is defined as:

$$\mathrm{Co} = \frac{U_{max}\Delta t}{\Delta x}, \tag{24}$$

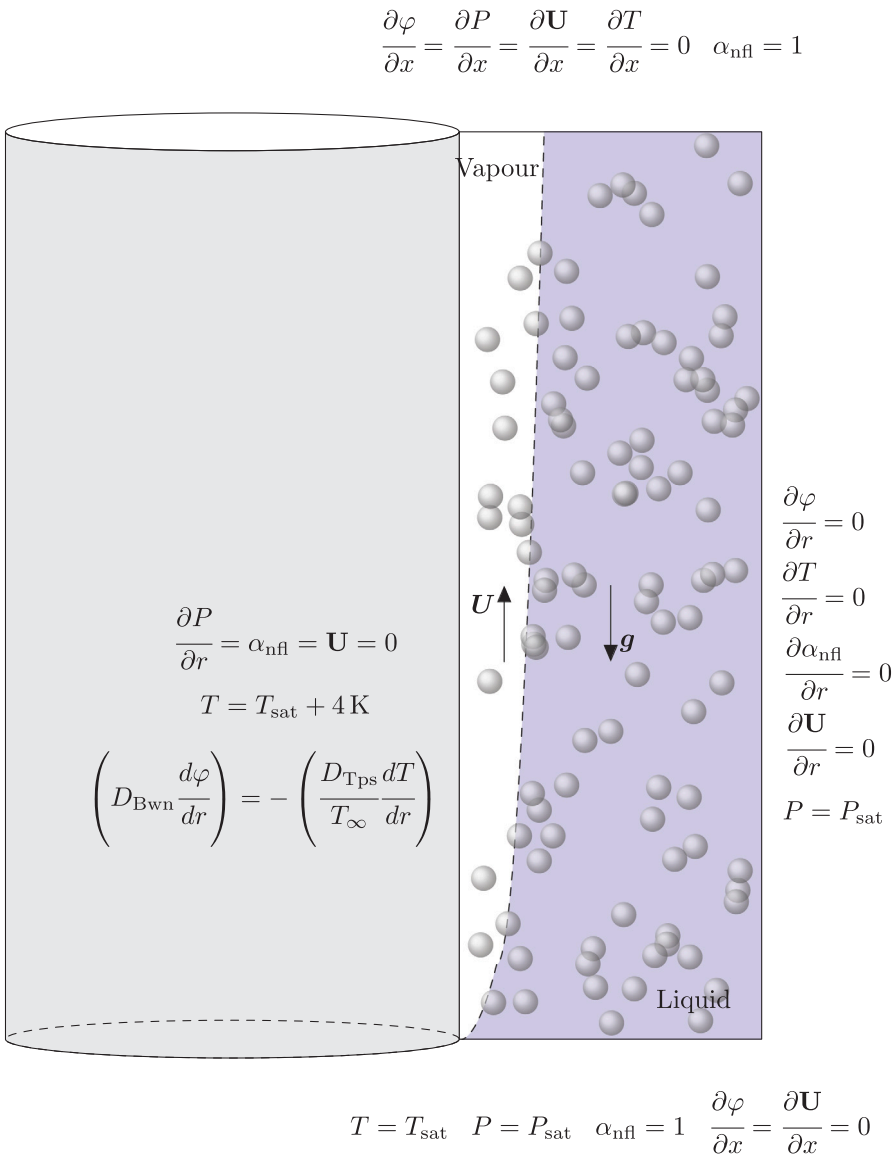


**Fig. 1.** Schematic showing the boundary constraints for laminar film boiling along a vertical interface. The white area represents the vapor film, the blue area indicates the liquid water at saturated temperature, and the gray cylinder has a supersaturated temperature of 4 K above the saturated temperature. Gray spheres, scattered randomly in both the vapor and liquid areas, represent the nanoparticles.

where Co denotes the Courant number, $U_{\max}$ is the peak flow velocity, $\Delta t$ represents the time step, and $\Delta x$ is the minimum dimension of the spatial grid. To ensure stability, the Courant number should remain below 1, ensuring that the simulation's physical information does not traverse more than one cell per time step, thereby maintaining the simulation's integrity.

As observed in the grid density independence study, a 300 × 300 grid with a simpleGrading of $15, 1, 1$ was used to enhance resolution at the wall, where the most significant gradients are found. From Fig. 5, it is apparent that the vapor–liquid interface in simulations with higher Courant numbers (such as Co = 0.5 and Co = 0.1) displays considerable disturbances. As the Courant number decreases, these fluctuations diminish, reaching minimal levels at Co = 0.005. This level of disturbance is nearly identical to that observed at a lower Courant number of Co = 0.001. Therefore, Co = 0.005 was chosen. This Courant number balances numerical stability and computational efficiency, following the CFL criterion. It minimizes discretization errors while ensuring an accurate representation of the fluid's temporal dynamics.

### 2.6. Dimensionless analysis of results

This study presents results using dimensionless numbers, enabling a normalized analysis of the physical phenomena. This method allows for effective comparisons across various scales and conditions.

The radial coordinates are normalized using the dimensionless parameter [84]:

$$r^* = \frac{r}{\delta_{\mathrm{refl}}}, \tag{25}$$

where $\delta_{\mathrm{refl}}$ is the reference length scale, presenting the vapor film thickness in the nanoparticle-free scenario when it reaches its steady state.

Time is dimensionally normalized as [84]:

$$t^* = \frac{\tau}{\mathrm{Pr}}, \quad \tau = \frac{t\mu_{\mathrm{g}}}{{\delta_{\mathrm{refl}}}^2 \rho_{\mathrm{g}}}. \tag{26}$$

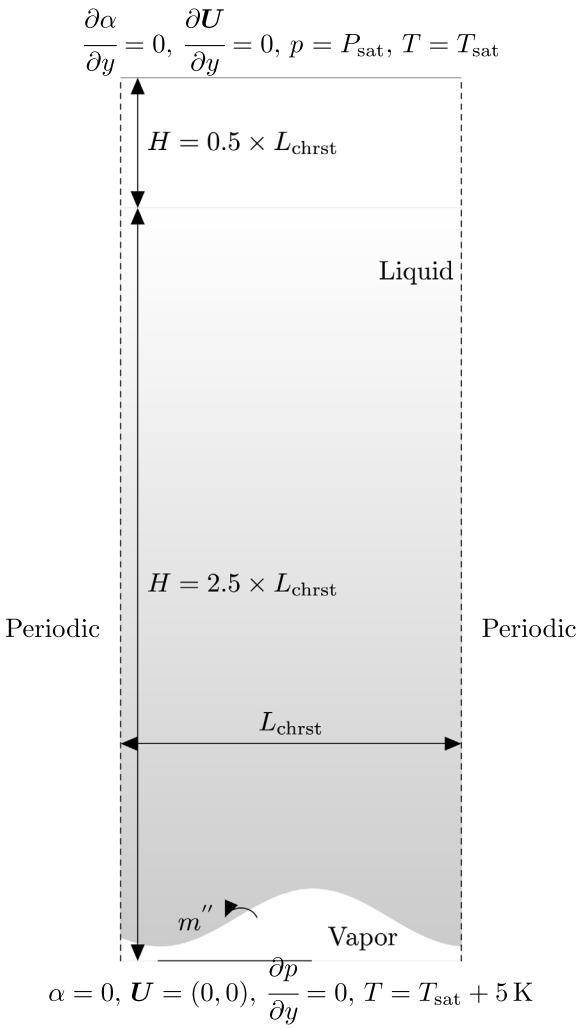


**Fig. 2.** Illustration of the boundary and initial conditions, and the configuration of the computational domain used in the two-dimensional film boiling case.

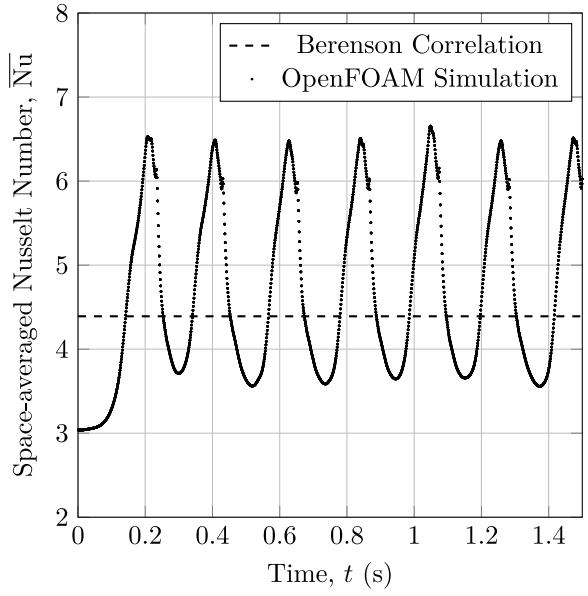


**Fig. 3.** Comparison of Nusselt numbers obtained from numerical simulations against Berenson's empirical model for two-dimensional film boiling in pure water.

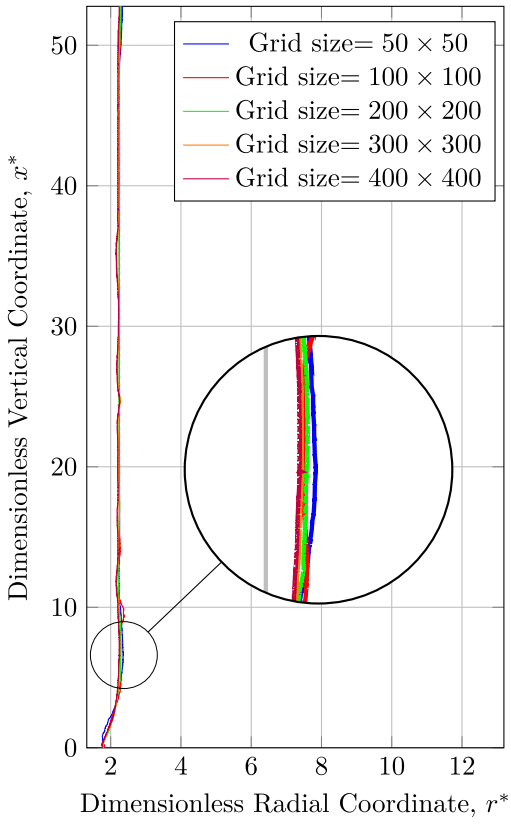


**Fig. 4.** Comparison of vapor film interface precision at a specific time instant across various mesh resolutions, utilizing a Courant number of 0.005.

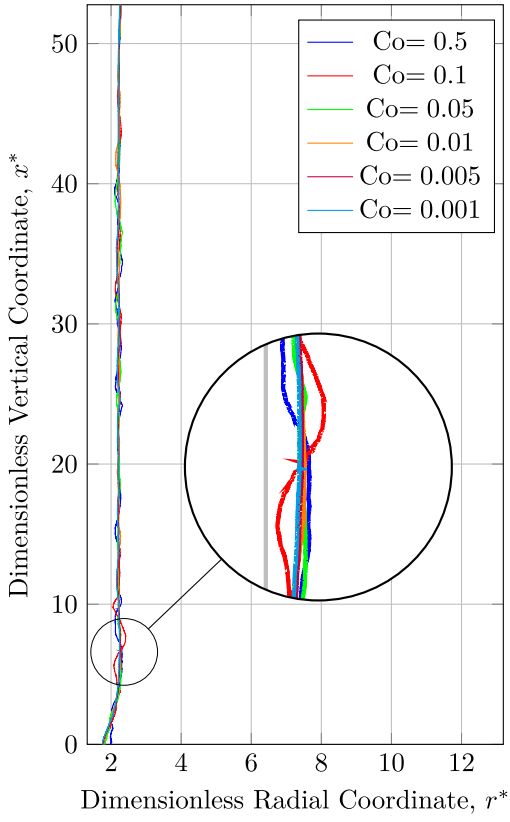


**Fig. 5.** Assessment of vapor film interface precision for differing Courant numbers at a constant time, employing a $300 \times 300$ mesh configuration.

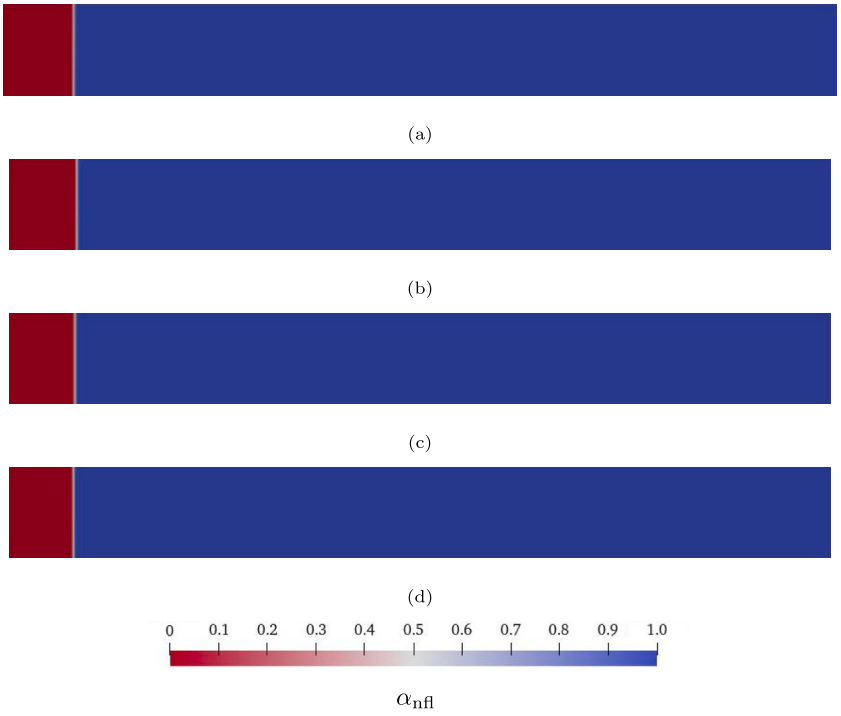


**Fig. 6.** Comparison of liquid nanofluid volume fraction ($\alpha_{nfl}$) at $t^* = 0.15$ for (a) size 5 nm, (b) size 10 nm, (c) size 30 nm, and (d) size 50 nm nanoparticles. Blue color indicates $\alpha_{nfl} = 1$, representing the liquid phase, while red color denotes $\alpha_{nfl} = 0$, signifying the vapor phase. The left boundary shows the heated cylinder wall.

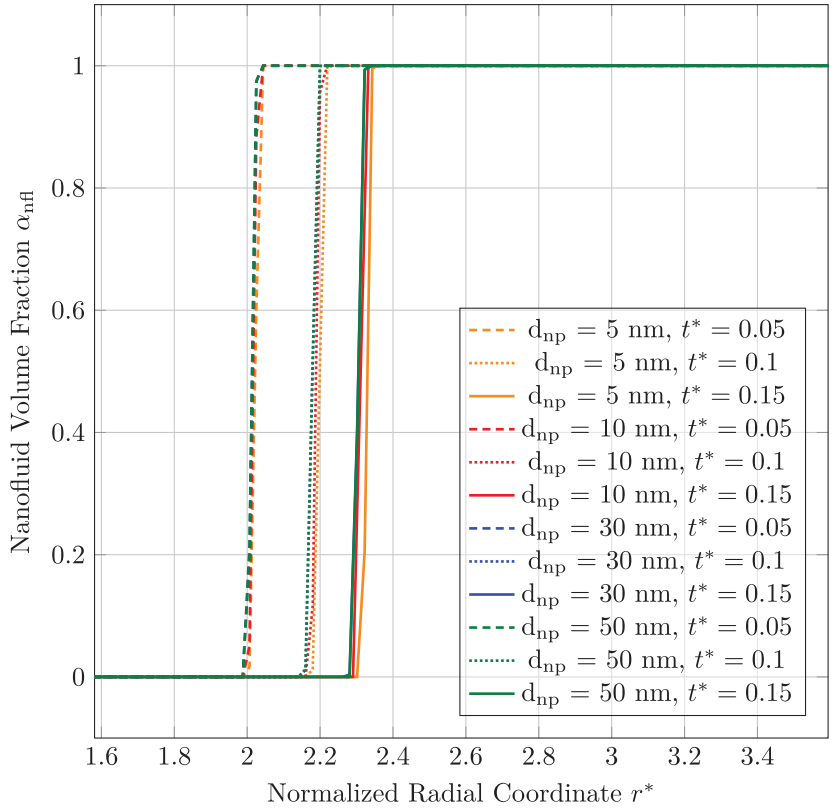


**Fig. 7.** Temporal evolution of the vapor–liquid interface as characterized by the nanofluid volume fraction for $Al_2O_3$ nanoparticles of sizes 5 nm, 10 nm, 30 nm, and 50 nm against the normalized radial coordinate ($r^*$). The data is captured at a constant axial position ($x^* = 40$) on the cylinder's surface for multiple non-dimensional times $t^*$.

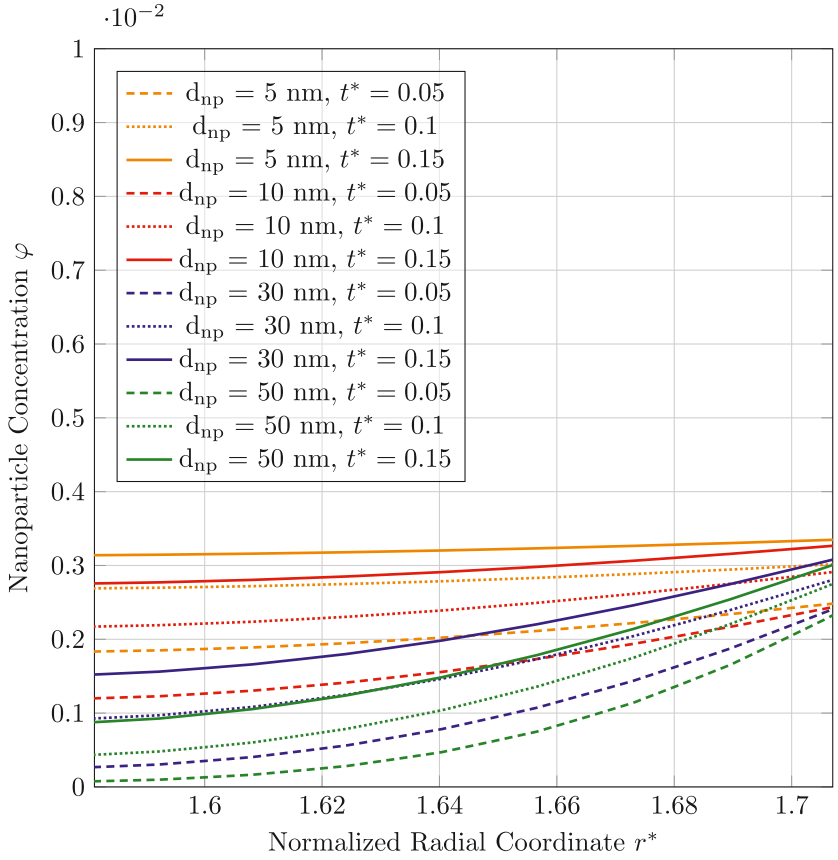


**Fig. 8.** Concentration profiles of $Al_2O_3$ nanoparticles of different sizes at and near the heated wall over time during film boiling. The data is captured at a constant axial position ($x^* = 40$) on the cylinder's surface for multiple non-dimensional times $t^*$.

The temperature field is normalized relative to the saturation temperature and the wall temperature:

$$T^* = \frac{T - T_{sat}}{T_{wall} - T_{sat}}. \tag{27}$$

The dimensionless Nusselt number, an indicator of heat transfer effectiveness, is normalized according to [84]:

$$\overline{Nu} = \frac{k(\varphi)}{\sqrt{t^*}} \frac{\partial T^*}{\partial r^*}\Big|_{r^*=R/\delta_{ref1}}, \tag{28}$$

where $k(\varphi)$ represents the thermal conductivity of the vapor nanofluid phase near the heating surface to the thermal conductivity of pure vapor.

A spatially-averaged normalized Nusselt number is used for a comprehensive understanding:

$$\overline{Nu}_{spav} = \frac{\int_0^L \left( \frac{k(\varphi)}{\sqrt{t^*}} \frac{\partial T^*}{\partial r^*}\Big|_{r^*=R/\delta_{ref1}} \right) dx}{L}. \tag{29}$$

This equation aggregates local Nusselt number variations along the length L and surface radius R of the vertical cylinder, providing an integrated perspective on heat transfer distribution.

## 3. Result and discussion

This study delves into the effects of varying sizes of $Al_2O_3$ nanoparticles (5 nm, 10 nm, 30 nm, and 50 nm) in water-based nanofluids on the heat transfer performance of film boiling along a vertical cylinder. This section discusses the influence of nanoparticle size on different aspects of flow, particularly examining aspects such as film thickness, nanoparticle concentration distribution, temperature distribution, and changes in essential thermophysical properties including thermal conductivity, viscosity, and surface tension. Additionaly, a part of the analysis is dedicated to exploring how these different nanoparticle sizes influence the Nusselt number. This dimensionless number is used for understanding the heat transfer performance in the film boiling process.

The contour representation of liquid nanofluid volume fraction depicted in Fig. 6 portrays the variation in vapor film thickness on a heated cylinder wall in the presence of nanofluid comprising nanoparticles of different diameters. The vapor film is represented by the extent of the red region adjacent to the wall. Due to the substantial elongation of the cylinder relative to the vapor film thickness, a full-length depiction encompassing the vapor film would compromise the interpretability of the figure. Consequently, only a limited yet illustrative segment of the vapor film and the adjacent liquid nanofluid along the cylinder wall is showcased.

A detailed assessment of Fig. 6 indicates that the vapor film exhibits the most considerable thickness when the nanofluid contains nanoparticles of 5 nm. A marginally diminished thickness is observed for the 10 nm nanoparticles. For nanoparticles with diameters of 30 nm and 50 nm, the vapor films exhibit almost identical thicknesses, though the film associated with the 30 nm nanoparticles is minimally thicker than that associated with the 50 nm ones. However, these thickness differences are less pronounced compared to those observed with nanoparticles of 5 nm and 10 nm diameters. A comprehensive analysis of this phenomenon is presented in Fig. 7, which provides a more detailed comparison across the nanoparticle size spectrum.

Fig. 7 presents nanofluid volume fraction profiles over time, using dimensionless radial coordinate ($r^*$) and dimensionless time ($t^*$), to explore the vapor–liquid interface dynamics during film boiling with $Al_2O_3$ nanoparticles of different sizes. The vapor–liquid interface, seen as a rapid transition from a volume fraction of zero to one, exhibits varying growth rates dependent on nanoparticle size.

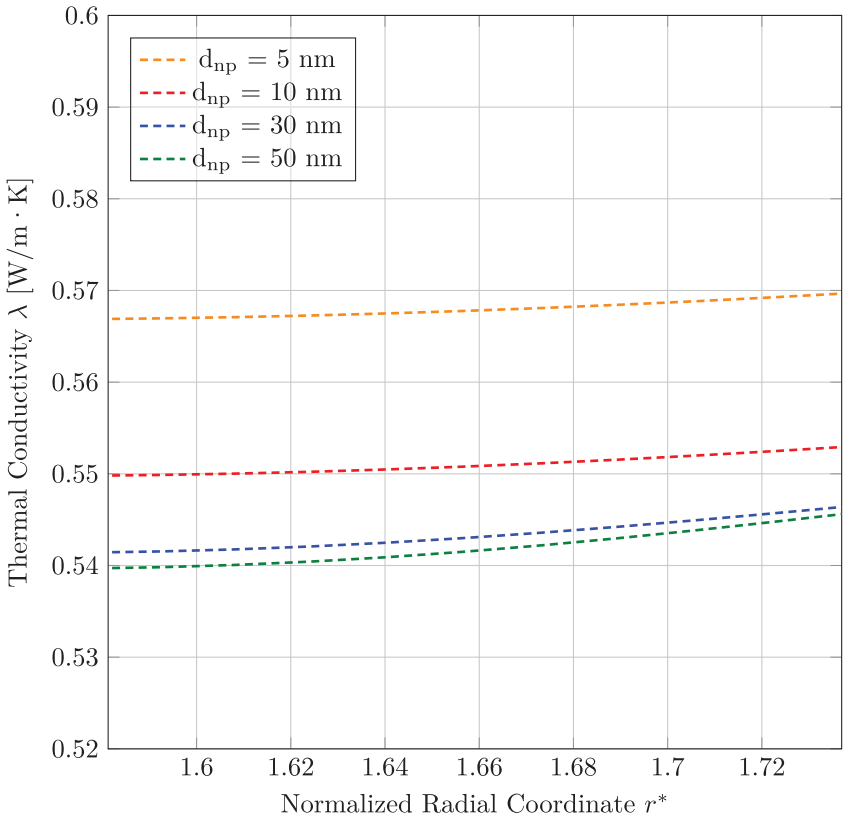


**Fig. 9.** Thermal conductivity variation with nanoparticle size at a non-dimensional time of $t^* = 0.15$. Probes are placed at a consistent axial position of $x^* = 40$.

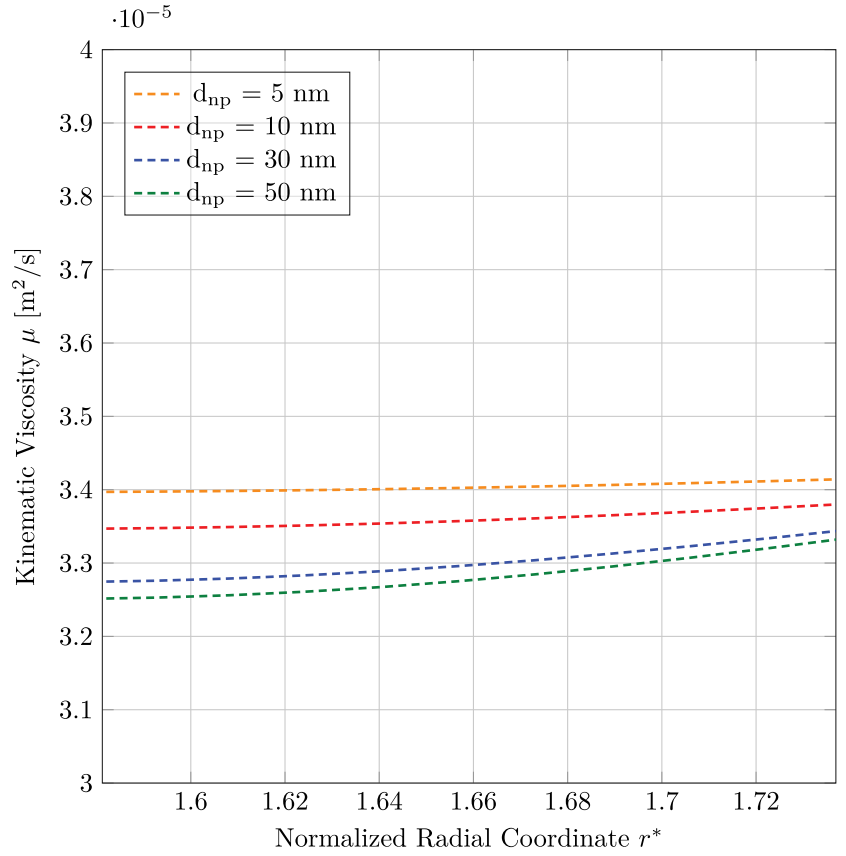


**Fig. 10.** The kinematic viscosity variations with nanoparticle size at a dimensionless time $t^* = 0.15$. Probes are placed at a consistent axial position of $x^* = 40$.

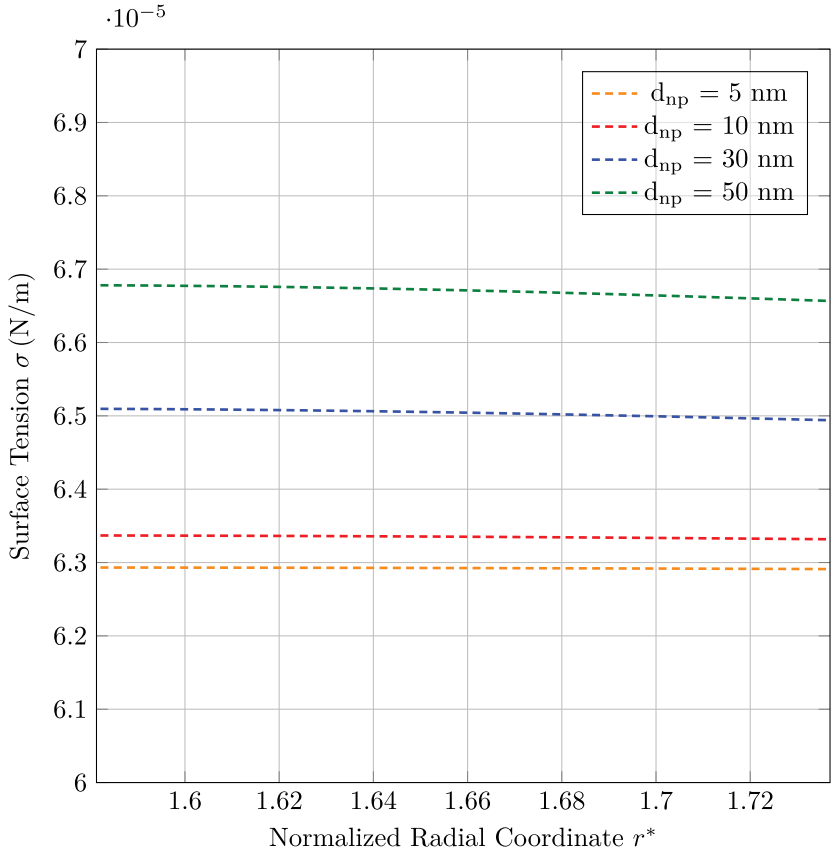


**Fig. 11.** Surface tension variation with nanoparticle size at a non-dimensional time $t^* = 0.15$. Probes are placed at a consistent axial position of $x^* = 40$.

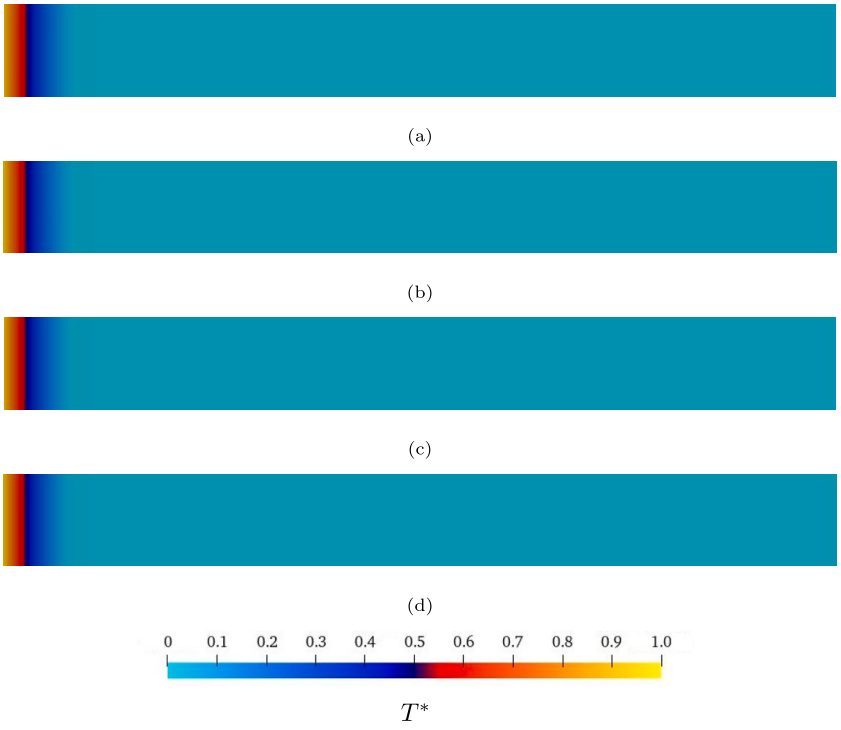


**Fig. 12.** Comparison of dimensionless temperature ($T^*$) profile at $t^* = 0.15$ for (a) size 5 nm, (b) size 10 nm, (c) size 30 nm, and (d) size 50 nm nanoparticles. The left boundary shows the heated cylinder wall.

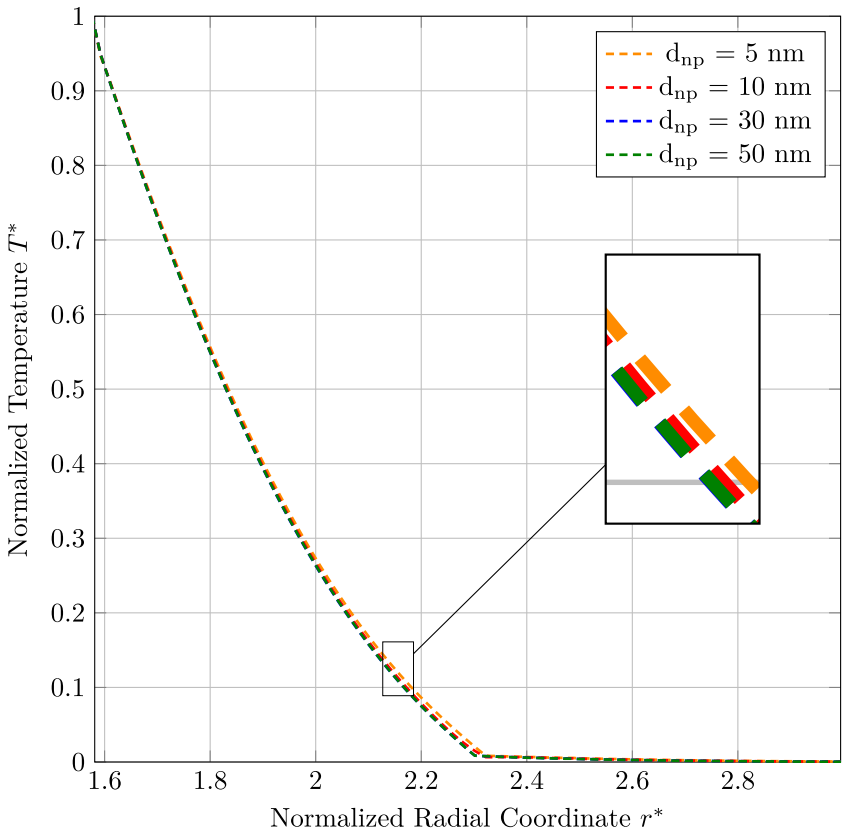


**Fig. 13.** Normalized temperature profiles during the boiling of nanofluid with varying nanoparticle sizes, observed at the dimensionless time $t^* = 0.15$, and recorded at an axial location $x^* = 40$ on the cylinder's vertical axis.

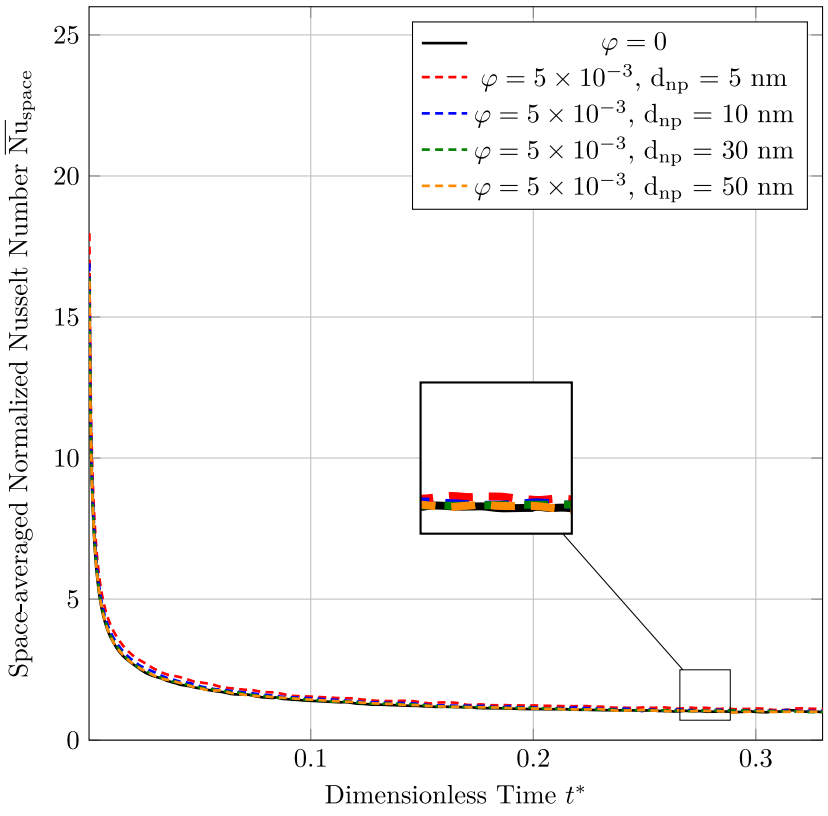


**Fig. 14.** Space-averaged normalized Nusselt number as a function of dimensionless time $t^*$ for nanofluids with nanoparticle sizes at the nanoparticle concentration of $\varphi = 5 \times 10^{-3}$.

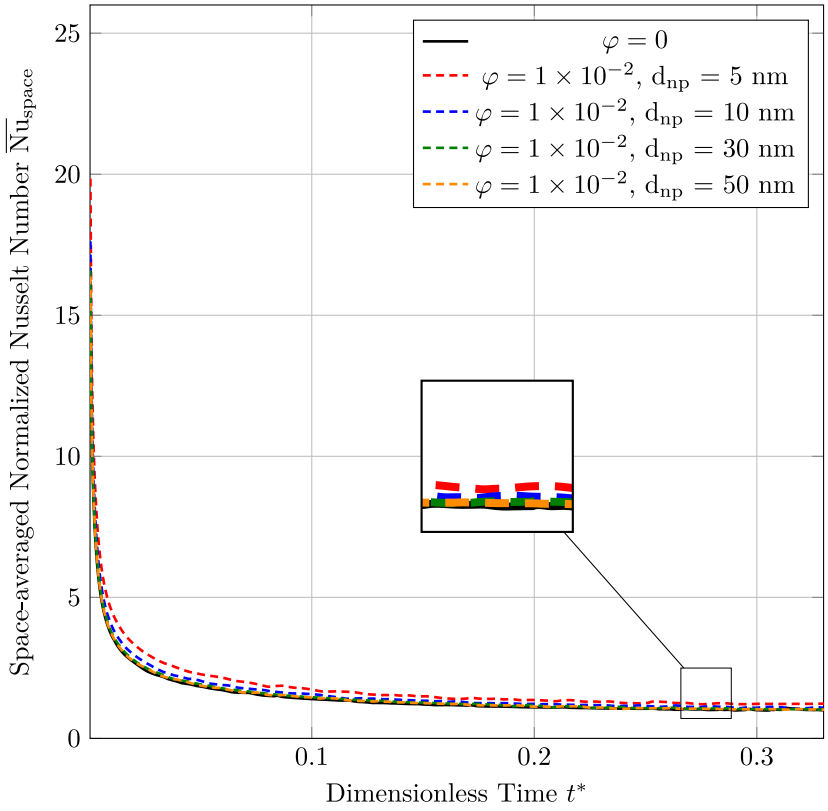


**Fig. 15.** Space-averaged normalized Nusselt number as a function of dimensionless time $t^*$ for nanofluids with nanoparticle sizes at the nanoparticle concentration of $\varphi = 1 \times 10^{-2}$.

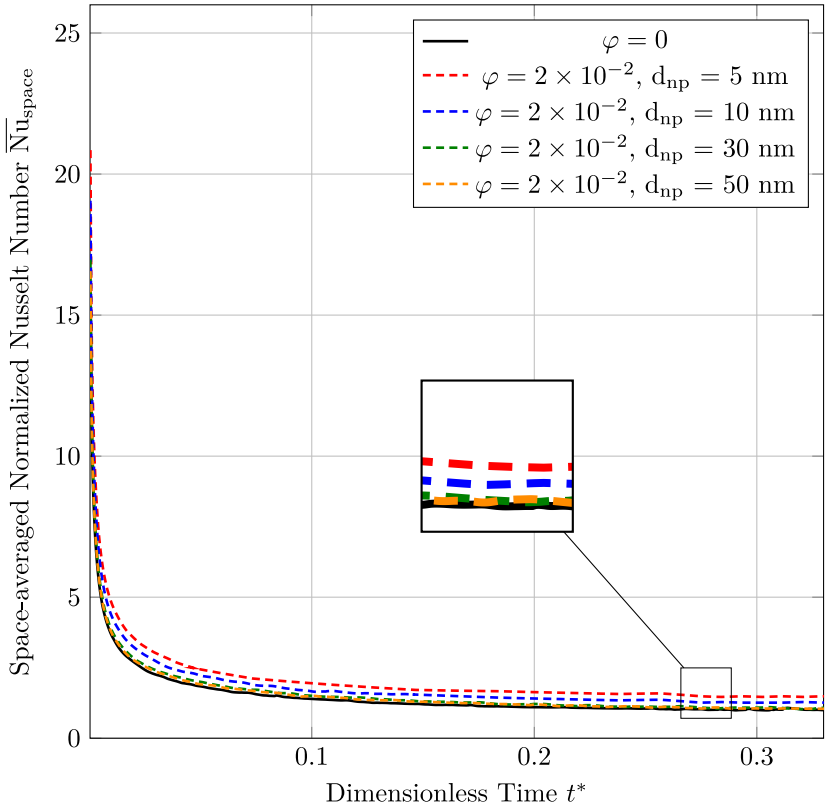


**Fig. 16.** Space-averaged normalized Nusselt number as a function of dimensionless time $t^*$ for nanofluids with nanoparticle sizes at the nanoparticle concentration of $\varphi = 2 \times 10^{-2}$.

With the progression of time, smaller nanoparticles (5 nm and 10 nm) demonstrate a quicker movement of the vapor–liquid interface, indicating a size-related enhancement in film growth rate. This accelerated interface growth, especially prominent with smaller nanoparticles, suggests a more vigorous boiling process, potentially leading to a higher rate of vapor generation. A contributing factor to this phenomenon is the increased surface area provided by smaller nanoparticles, which promotes more efficient heat transfer due to the larger interface available for energy exchange.

In contrast, the impact of size on the growth rate of the interface for larger nanoparticles (30 nm and 50 nm) appears more subdued. The similar behavior of the interface for both 30 nm and 50 nm particles might indicate a threshold beyond which the effect of nanoparticle size on vapor film dynamics stabilizes, and reach a plateau as particle size increases.

The concentration profiles of $Al_2O_3$ nanoparticles of different sizes are depicted in Fig. 8, illustrating their concentration adjacent to the heated wall in this film boiling scenario. The initial uniform concentration of nanoparticles in the liquid nanofluid is $1 \times 10^{-2}$.

These profiles reveal that smaller nanoparticle sizes, compared to larger nanoparticles, correspond to higher concentrations at and near the wall. This trend becomes increasingly apparent over time, as observed at various non-dimensional times, $t^*$. The emergent patterns imply that finer nanoparticles have a more significant effect on the boiling heat transfer process.

The proximity of the heated wall plays a pivotal role in the boiling phenomena of nanofluids, directly influencing the heat transfer efficiency as characterized by the Nusselt number. Fig. 9, Fig. 10, and Fig. 11 showcase the variations in thermal conductivity, viscosity, and surface tension adjacent to the heated surface. These thermophysical properties are crucial for determining the heat transfer and fluid dynamic behavior of nanofluids and are subject to modifications based on the size-specific attributes of the dispersed nanoparticles.

Fig. 9 presents the impact of nanoparticle size on thermal conductivity, depicted across the normalized radial coordinate for a given non-dimensional time step, $t^*$. It is observed that the thermal conductivity of the nanofluid is influenced by the size of the dispersed nanoparticles. Specifically, smaller nanoparticles contribute to an increase in thermal conductivity. In contrast, the augmentation in thermal conductivity diminishes with larger nanoparticles.

Kinematic viscosity profiles for nanofluids containing various sizes of nanoparticles are elucidated in Fig. 10. These profiles are crucial for understanding the flow dynamics in film boiling applications, where viscosity plays a significant role.

The data presented in Fig. 10 reveals that kinematic viscosity increases inversely with nanoparticle size. This trend implies that smaller nanoparticles disrupt the fluid's laminar flow more than their larger counterparts, resulting in increased viscous forces. The findings suggest a trade-off between the thermal conductivity benefits provided by smaller nanoparticles and their impact on increasing viscosity, which could translate to higher energy requirements for fluid circulation in practical heat transfer systems. Notably, the 5 nm nanoparticles demonstrate the most increase in viscosity, potentially harmfully affecting the fluidity. Conversely, larger nanoparticles, particularly those of 30 nm and 50 nm, present less impact on viscosity increase, indicating that the size effect on viscosity may plateau beyond a certain nanoparticle diameter.

The implications of these figures are significant for the design and application of nanofluid-based cooling systems. The optimal nanoparticle size for such applications would be one that balances the dual objectives of improved thermal conductivity and manageable viscosity, ensuring enhanced heat transfer performance without incurring prohibitive pumping costs.

Surface tension is another crucial factor affecting the boiling behavior of nanofluids, as it directly influences bubble nucleation and stability. The dependency of surface tension on nanoparticle size is demonstrated in Fig. 11, with the assessment conducted at a non-dimensional time $t^* = 0.15$.

Analysis of the data presented in Fig. 11 reveals that nanofluids with smaller nanoparticles exhibit a reduction in surface tension. The most pronounced decrease is observed in nanofluids with the smallest nanoparticles (5 nm). Conversely, as the nanoparticle size increases, the influence on surface tension becomes less intense.

The implications of reduced surface tension are multifaceted within the boiling process. With smaller nanoparticles, the facilitated bubble formation and release could lead to an improved boiling efficiency. Meanwhile, the subtle effect of larger nanoparticles on surface tension points to a marginal impact on the boiling dynamics.

Fig. 12 depicts the dimensionless temperature ($T^*$) distributions within the studied domain, differentiated by the nanoparticle sizes. From the heated surface outward, the temperature decreases to reach the saturation temperature of the liquid nanofluid. The study progresses by examining Fig. 13, with the goal of uncovering more pronounced distinctions and additional insights.

Fig. 13 showcases the normalized temperature profiles for nanofluids comprising nanoparticles of various sizes (5 nm, 10 nm, 30 nm, and 50 nm), illustrating the thermal gradients during the boiling process. Derived from line probe measurements, these profiles reveal a temperature decrement from the wall towards the fluid's bulk. The observed convergence in profiles for larger nanoparticles (30 nm and 50 nm) implies a size beyond which the temperature profiles become relatively close. The transition from a steep near-wall gradient to a more leveled curve away from the wall indicates the expansion of the thermal boundary layer, a phenomenon pivotal to nanofluid boiling heat transfer.

The influence of nanoparticle diameter and volumetric concentration on the space-averaged normalized Nusselt number, $\overline{Nu}_{spav}$, is shown in Figs. 14, 15, and 16. The study assesses the enhancement in heat transfer of nanofluids with nanoparticle diameters of 5 nm, 10 nm, 30 nm, and 50 nm, at varying nanoparticle concentrations, $\varphi$. The enhancements in the Nusselt number are quantified at steady-state conditions and are relative to the base fluid without nanoparticles, serving as the reference point for comparison.

At a nanoparticle concentration of $\varphi = 5 \times 10^{-3}$ (Fig. 14), enhancements in the Nusselt number relative to the pure fluid are observed to be 5%, 4.62%, 4.12%, and 1.07% for nanoparticle diameters of 5 nm, 10 nm, 30 nm, and 50 nm, respectively. These findings indicate that at lower concentrations, the impact of even smaller nanoparticles on heat transfer efficiency may diminish, as evidenced by the closely aligned enhancements across the 5 nm, 10 nm, and 30 nm diameters. This illustrates a nuanced perspective that, although smaller nanoparticles can significantly affect thermal performance, their impact at lower concentrations tends to be less marked, leading to more subtle distinctions in heat transfer enhancements among various nanoparticle sizes.

As the concentration increases to $\varphi = 1 \times 10^{-2}$ (Fig. 15), the impact of nanoparticle size on heat transfer efficiency becomes increasingly evident. For nanoparticle diameters of 5 nm, 10 nm, 30 nm, and 50 nm, the enhancements in the Nusselt number relative to pure fluid are recorded at 10%, 7.30%, 4.99%, and 2.88% respectively. These findings underscore that higher concentrations magnify the influence of nanoparticle size on thermal performance. Notably, while 5 nm nanoparticles demonstrate the most substantial heat transfer improvement, the emergence of a significant performance differentiation for 10 nm nanoparticles relative to the larger 30 nm and 50 nm sizes is observed. This delineation suggests that nanoparticles with diameters of 10 nm and smaller become effective in augmenting the Nusselt number, highlighting their advantage for enhancing heat transfer efficiency at elevated nanoparticle concentrations.

At the highest analyzed nanoparticle concentration of $\varphi = 2 \times 10^{-2}$ (Fig. 16), the observed enhancements in the Nusselt number relative to pure fluid for nanoparticles with diameters of 5 nm and 10 nm are significant, at 48.29% and 25.82% respectively. This underlines the substantial impact of smaller nanoparticles on the enhancement of boiling heat transfer efficiency. In contrast, for nanoparticles with diameters of

30 nm and 50 nm, the increases in the Nusselt number are more modest, at 7.88% and 5.10% respectively. These observations, consistent across Figs. 14, 15, and 16, suggest that the influence of nanoparticle size on the Nusselt number begins to diminish for larger diameters, indicating a diminishing return on heat transfer enhancement with increasing nanoparticle size.

## 4. Conclusion

The investigation into the impact of nanoparticle size on the film boiling of nanofluids has elucidated several key aspects of thermal transfer and fluid dynamics. This study specifically focused on $Al_2O_3$ nanoparticles of varying sizes dispersed in water, examining the consequent effects on the boiling process along a vertical cylinder. Advanced computational simulations, facilitated by the Continuous-Species-Transfer method within a Computational Multi-Fluid Dynamics framework, have significantly deepened the comprehension of the impact of nanoparticle size on the thermophysical attributes and boiling heat transfer efficiency of nanofluids. The findings can be summarized as follows:

- Nanoparticles of 5 nm and 10 nm diameters significantly expedite the vapor–liquid interface expansion, suggesting an efficient boiling process with enhanced vapor generation and cooling efficiency due to increased surface area and interactions at the thermal boundary layer.
- Larger nanoparticles (30 nm and 50 nm) show a diminished impact on interface growth rate, indicating a plateauing effect of size on boiling heat transfer beyond a certain threshold.
- Thermophysical properties, namely thermal conductivity, viscosity, and surface tension, are markedly influenced by nanoparticle size. Smaller nanoparticles improve thermal conductivity and reduce surface tension, beneficial for heat transfer and bubble formation, respectively, but inversely increase kinematic viscosity, potentially complicating fluid dynamics.
- A nuanced trade-off exists between the thermal benefits provided by smaller nanoparticles and their impact on viscous resistance, underscoring the need for optimization in nanofluid design to balance enhanced heat transfer with the energy requirements for fluid circulation.
- The investigation demonstrates that nanoparticle diameter and concentration directly affect the space-averaged normalized Nusselt number, with smaller nanoparticles (5 nm and 10 nm) offering substantial improvements in heat transfer efficiency at higher concentrations. This highlights the critical role of nanoparticle size and concentration in enhancing boiling heat transfer.

In conclusion, the study affirms the pivotal role of nanoparticle size in dictating the boiling heat transfer performance of nanofluids. Smaller nanoparticles (5 nm and 10 nm) are identified as significantly beneficial in improving boiling heat transfer efficiency, particularly at higher concentrations, through mechanisms, some of which may involve enhanced thermal conductivity and reduced surface tension. However, the increased kinematic viscosity presented by smaller nanoparticles poses a challenge, necessitating a balanced approach in nanofluid formulation to optimize thermal management capabilities without incurring prohibitive pumping costs. These insights offer a valuable foundation for future research and the development of nanofluid-based thermal management systems, emphasizing the importance of nanoparticle size selection to achieve desired thermal performance outcomes.

## CRediT authorship contribution statement

**A. Yahyaee:** Writing – review & editing, Writing – original draft, Visualization, Validation, Software, Methodology, Investigation, Formal analysis, Data curation, Conceptualization. **P. Vatankhah:** Investigation, Software, Visualization, Writing – review & editing. **H. Sørensen:** Conceptualization, Project administration, Resources, Software.

## Declaration of competing interest

The authors declare that they have no known competing financial interests or personal relationships that could have appeared to influence the work reported in this paper.

## Data availability

No data was used for the research described in the article.

## References

[1] A.Y. Nujukambari, A.S. Bahman, J. Hærvig, H. Sørensen, A review: New designs of heat sinks for flow boiling cooling, in: 2019 25th International Workshop on Thermal Investigations of ICs and Systems, THERMINIC, IEEE, 2019, pp. 1–6.
[2] D. Wang, P. Cheng, Effects of nanoparticles' wettability on vapor bubble coalescence in saturated pool boiling of nanofluids: A lattice Boltzmann simulation, Int. J. Heat Mass Transfer 154 (2020) 119669.
[3] M.S. Kamel, F. Lezsovits, Enhancement of pool boiling heat transfer performance using dilute cerium oxide/water nanofluid: An experimental investigation, Int. Commun. Heat Mass Transfer 114 (2020) 104587.
[4] M. Huang, H. Borzoei, A. Abdollahi, Z. Li, A. Karimipour, Effect of concentration and sedimentation on boiling heat transfer coefficient of GNPs-SiO2/deionized water hybrid Nanofluid: An experimental investigation, Int. Commun. Heat Mass Transfer 122 (2021) 105141.
[5] G. Liang, H. Yang, J. Wang, S. Shen, Assessment of nanofluids pool boiling critical heat flux, Int. J. Heat Mass Transfer 164 (2021) 120403.
[6] Y. Chen, S. Fu, J. Guo, X. Liu, D. He, Study of pool boiling heat transfer of nanofluid in the PCD electrical fields, Int. Commun. Heat Mass Transfer 137 (2022) 106213.
[7] J. Du, Y. Wang, W. Yang, J. Wang, Z. Cao, B. Sundén, Effect of nanoparticle concentration and surfactants on nanofluid pool boiling, Int. J. Heat Mass Transfer 221 (2024) 125080.
[8] F.J. do Nascimento, T.A. Moreira, G. Ribatski, Flow boiling critical heat flux of DI-water and nanofluids inside smooth and nanoporous round microchannels, Int. J. Heat Mass Transfer 139 (2019) 240–253.
[9] Y. Wang, K. Deng, J.M. Wu, G. Su, S. Qiu, A mechanism of heat transfer enhancement or deterioration of nanofluid flow boiling, Int. J. Heat Mass Transfer 158 (2020) 119985.
[10] H.I. Mohammed, D. Giddings, G.S. Walker, P. Talebizadehsardari, J.M. Mahdi, Thermal behaviour of the flow boiling of a complex nanofluid in a rectangular channel: An experimental and numerical study, Int. Commun. Heat Mass Transfer 117 (2020) 104773.
[11] X. Yin, C. Hu, M. Bai, J. Lv, An investigation on the heat transfer characteristics of nanofluids in flow boiling by molecular dynamics simulations, Int. J. Heat Mass Transfer 162 (2020) 120338.
[12] M. McCord, C.S. Brooks, Experimental comparison of the rewet phenomenon in transient and stable film boiling in low pressure and low flow conditions, Int. J. Heat Mass Transfer 209 (2023) 124099.
[13] K.R. Kunniyoor, V. Kunniyoor, P. Ghosh, Development of constitutive relations for predicting film boiling crisis in bare and inner wall coated cryogenic tubes with a low-thermal conductive layer for heat transfer enhancement, Int. J. Heat Mass Transfer 222 (2024) 125112.
[14] J. Li, Z. Zhang, Y. Zhang, R. Zhao, H. Cui, T. Zhai, W. Liu, Z. Liu, High heat flux dissipation of membrane-venting heat sink with thin film boiling, Int. J. Heat Mass Transfer 221 (2024) 125078.
[15] K. Guo, H. Li, Y. Feng, T. Wang, J. Zhao, Enhancement of non-uniform magnetic field on saturated film boiling of magnetic nanofluid (MNF), Int. J. Heat Mass Transfer 143 (2019) 118594.
[16] K. Guo, H. Li, Y. Feng, T. Wang, J. Zhao, Numerical simulation of magnetic nanofluid (MNF) film boiling using the VOSET method in presence of a uniform magnetic field, Int. J. Heat Mass Transfer 134 (2019) 17–29.
[17] A. Sedaghatkish, J. Sadeghiseraji, M.Y.A. Jamalabadi, Numerical simulation of magnetic nanofluid (MNF) film boiling on cylindrical heated magnet using phase field method, Int. J. Heat Mass Transfer 152 (2020) 119546.
[18] R. Santos, A.P. Ribeiro, A.L. Moreira, A.S.O. Moita, Effect of alumina nanofluids on bubble dynamics and heat transfer under quiescent conditions, Int. J. Thermofluids 15 (2022) 100168.
[19] A.A. Eidan, A. Alsahlani, M.J. Alshukri, A.I. Alsabery, Experimental investigation of a solar evacuated tube collector embedded with a heat pipe using different nanofluids and controlled mechanical exciting pulsations, Int. J. Thermofluids 20 (2023) 100415.
[20] J.C. Maxwell, A Treatise on Electricity and Magnetism, vol. 1, Clarendon Press, 1873.
[21] G. Liang, I. Mudawar, Review of single-phase and two-phase nanofluid heat transfer in macro-channels and micro-channels, Int. J. Heat Mass Transfer 136 (2019) 324–354.

[22] M. Awais, N. Ullah, J. Ahmad, F. Sikandar, M.M. Ehsan, S. Salehin, A.A. Bhuiyan, Heat transfer and pressure drop performance of Nanofluid: A state-of- the-art review, Int. J. Thermofluids 9 (2021) 100065.
[23] S.U.S. Choi, J.A. Eastman, Enhancing Thermal Conductivity of Fluids with Nanoparticles, Technical Report, Argonne National Lab.(ANL), Argonne, IL (United States), 1995.
[24] R.B. Ganvir, P.V. Walke, V.M. Kriplani, Heat transfer characteristics in nanofluid—A review, Renew. Sustain. Energy Rev. 75 (2017) 451–460.
[25] F. Zhang, A.M. Jacobi, Aluminum surface wettability changes by pool boiling of nanofluids, Colloids Surf. A 506 (2016) 438–444.
[26] A. Pare, S.K. Ghosh, Surface qualitative analysis and ANN modelling for pool boiling heat transfer using Al2O3-water based nanofluids, Colloids Surf. A 610 (2021) 125926.
[27] A. Kujawska, R. Mulka, S. Hamze, G. Żyła, B. Zajaczkowski, M.H. Buschmann, P. Estellé, The effect of boiling in a thermosyphon on surface tension and contact angle of silica and graphene oxide nanofluids, Colloids Surf. A 627 (2021) 127082.
[28] P.O. Sharma, D.R. Unune, Augmentation of pool boiling performance using Ag/ZnO hybrid nanofluid over EDM assisted robust heater surface modification, Colloids Surf. A 655 (2022) 130150.
[29] A. Yahyaee, J. Hærvig, H. Sørensen, Nanoparticle migration in nanofluid film boiling: A numerical analysis using the continuous-species-transfer method, Int. J. Heat Mass Transfer 224 (2024) 125344.
[30] A. Yahyaee, Influence of nanoparticle shapes in nanofluid film boiling on vertical cylinders: A numerical study, Int. J. Thermofluids 22 (2024) 100631.
[31] M. Borzuei, Z. Baniamerian, Role of nanoparticles on critical heat flux in convective boiling of nanofluids: Nanoparticle sedimentation and Brownian motion, Int. J. Heat Mass Transfer 150 (2020) 119299.
[32] G.-S. Wang, B. Song, Z.-H. Liu, Operation characteristics of cylindrical miniature grooved heat pipe using aqueous CuO nanofluids, Exp. Therm Fluid Sci. 34 (8) (2010) 1415–1421.
[33] M.B.B. Esfahani, S.M. Sajadi, N.H. Abu-Hamdeh, S. Bezzina, A. Abdollahi, A. Karimipour, F. Ghaemi, D. Baleanu, The effect of sedimentation phenomenon of the additives silver nano particles on water pool boiling heat transfer coefficient: A comprehensive experimental study, J. Mol. Liq. 345 (2022) 117891.
[34] S. Rashidi, O. Mahian, E.M. Languri, Applications of nanofluids in condensing and evaporating systems: A review, J. Therm. Anal. Calorim. 131 (2018) 2027–2039.
[35] V.P. Carey, Liquid-Vapor Phase-Change Phenomena: An Introduction to the Thermophysics of Vaporization and Condensation Processes in Heat Transfer Equipment, CRC Press, 2020.
[36] X. Yin, C. Hu, M. Bai, J. Lv, Effects of depositional nanoparticle wettability on explosive boiling heat transfer: A molecular dynamics study, Int. Commun. Heat Mass Transfer 109 (2019) 104390.
[37] S. Vafaei, A. Purkayastha, A. Jain, G. Ramanath, T. Borca-Tasciuc, The effect of nanoparticles on the liquid–gas surface tension of Bi2Te3 nanofluids, Nanotechnology 20 (18) (2009) 185702.
[38] J. Ally, M. Kappl, H.-J. Butt, A. Amirfazli, Detachment force of particles from air-liquid interfaces of films and bubbles, Langmuir 26 (23) (2010) 18135–18143.
[39] E. Abedini, A. Behzadmehr, S.M. Sarvari, S.H. Mansouri, Numerical investigation of subcooled flow boiling of a nanofluid, Int. J. Therm. Sci. 64 (2013) 232–239.
[40] S.N. Shoghl, M. Bahrami, M.K. Moraveji, Experimental investigation and CFD modeling of the dynamics of bubbles in nanofluid pool boiling, Int. Commun. Heat Mass Transfer 58 (2014) 12–24.
[41] C. Qi, Y.L. Wan, C.Y. Li, D.T. Han, Z.H. Rao, Experimental and numerical research on the flow and heat transfer characteristics of TiO2-water nanofluids in a corrugated tube, Int. J. Heat Mass Transfer 115 (2017) 1072–1084.
[42] A. Abdollahi, H.A. Mohammed, S.M. Vanaki, A. Osia, M.R. Golbahar Haghighi, Fluid flow and heat transfer of nanofluids in microchannel heat sink with V-type inlet/outlet arrangement, Alex. Eng. J. 56 (1) (2017) 161–170.
[43] H.I. Mohammed, D. Giddings, G.S. Walker, CFD simulation of a concentrated salt nanofluid flow boiling in a rectangular tube, Int. J. Heat Mass Transfer 125 (2018) 218–228.
[44] G. Li, X. Fang, Numerical simulation on the boiling flow patterns of Al2O3-water nanofluid in micro/minichannel under different hypergravity levels and directions, Int. J. Aerosp. Eng. 2021 (2021).
[45] S. Zaboli, H. Alimoradi, M. Shams, Numerical investigation on improvement in pool boiling heat transfer characteristics using different nanofluid concentrations, J. Therm. Anal. Calorim. (2022) 1–18.
[46] M. Bahiraei, N. Mazaheri, M.R. Daneshyar, A. Mwesigye, Two-phase simulation of irreversibilities for Ag–water nanofluid flow inside an elliptical pin-fin heat sink: Entropy generation and exergy considerations, Powder Technol. 409 (2022) 117723.
[47] J. Buongiorno, Convective Transport in Nanofluids, 2006.
[48] C. Yang, W. Li, A. Nakayama, Convective heat transfer of nanofluids in a concentric annulus, Int. J. Therm. Sci. 71 (2013) 249–257.
[49] A. Malvandi, S.A. Moshizi, E.G. Soltani, D.D. Ganji, Modified Buongiorno's model for fully developed mixed convection flow of nanofluids in a vertical annular pipe, Comput. & Fluids 89 (2014) 124–132.
[50] A. Malvandi, S. Heysiattalab, D.D. Ganji, Thermophoresis and Brownian motion effects on heat transfer enhancement at film boiling of nanofluids over a vertical cylinder, J. Mol. Liq. 216 (2016) 503–509.
[51] F. Hedayati, G. Domairry, Effects of nanoparticle migration and asymmetric heating on mixed convection of TiO2–H2O nanofluid inside a vertical microchannel, Powder Technol. 272 (2015) 250–259.
[52] F. Hedayati, G. Domairry, Nanoparticle migration effects on fully developed forced convection of TiO2–water nanofluid in a parallel plate microchannel, Particuology 24 (2016) 96–107.
[53] A. Malvandi, Anisotropic behavior of magnetic nanofluids (MNFs) at film boiling over a vertical cylinder in the presence of a uniform variable-directional magnetic field, Powder Technol. 294 (2016) 307–314.
[54] M. Wang, P.S. Dobson, M.C. Paul, Numerical investigation of nanofluid deposition in a microchannel cooling system, Powder Technol. 425 (2023) 118582.
[55] H. Peng, G. Ding, H. Hu, W. Jiang, Effect of nanoparticle size on nucleate pool boiling heat transfer of refrigerant/oil mixture with nanoparticles, Int. J. Heat Mass Transfer 54 (9–10) (2011) 1839–1850.
[56] R.R. Souza, J.C. Passos, E.M. Cardoso, Influence of nanoparticle size and gap size on nucleate boiling using HFE7100, Exp. Therm. Fluid Sci. 59 (2014) 195–201.
[57] Y. Hu, H. Li, Y. He, Z. Liu, Y. Zhao, Effect of nanoparticle size and concentration on boiling performance of SiO2 nanofluid, Int. J. Heat Mass Transfer 107 (2017) 820–828.
[58] T. Sayahi, M. Bahrami, Investigation on the effect of type and size of nanoparticles and surfactant on pool boiling heat transfer of nanofluids, J. Heat Transfer 138 (3) (2016) 031502.
[59] L. Liu, V. Stetsyuk, K.J. Kubiak, Y.F. Yap, A. Goharzadeh, J.C. Chai, Nanoparticles for convective heat transfer enhancement: Heat transfer coefficient and the effects of particle size and zeta potential, Chem. Eng. Commun. 206 (6) (2019) 761–771.
[60] C. Kunkelmann, P. Stephan, CFD simulation of boiling flows using the volume-of-fluid method within OpenFOAM, Numer. Heat Transf. A: Appl. 56 (8) (2009) 631–646.
[61] H. Rusche, Computational Fluid Dynamics of Dispersed Two-Phase Flows at High Phase Fractions, University of London, 2002.
[62] J.U. Brackbill, D.B. Kothe, C. Zemach, A continuum method for modeling surface tension, J. Comput. Phys. 100 (2) (1992) 335–354.
[63] J. Klostermann, K. Schaake, R. Schwarze, Numerical simulation of a single rising bubble by VOF with surface compression, Internat. J. Numer. Methods Fluids 71 (8) (2013) 960–982.
[64] N. Samkhaniani, M.R. Ansari, Numerical simulation of bubble condensation using CF-VOF, Prog. Nucl. Energy 89 (2016) 120–131.
[65] H.G. Weller, A New Approach to VOF–Based Interface Capturing Methods for Incompressible, Compressible and Cavitating Flow, Technical Report, OpenCFD Limited, 2006.
[66] E. Olsson, G. Kreiss, A conservative level set method for two phase flow, J. Comput. Phys. 210 (1) (2005) 225–246.
[67] H. Marschall, K. Hinterberger, C. Schüler, F. Habla, O. Hinrichsen, Numerical simulation of species transfer across fluid interfaces in free-surface flows using OpenFOAM, Chem. Eng. Sci. 78 (2012) 111–127.
[68] S. Hardt, F. Wondra, Evaporation model for interfacial flows based on a continuum-field representation of the source terms, J. Comput. Phys. 227 (11) (2008) 5871–5895.
[69] Y. Xuan, W. Roetzel, Conceptions for heat transfer correlation of nanofluids, Int. J. Heat Mass Transf. 43 (19) (2000) 3701–3707.
[70] M. Corcione, Empirical correlating equations for predicting the effective thermal conductivity and dynamic viscosity of nanofluids, Energy Convers. Manag. 52 (1) (2011) 789–793, http://dx.doi.org/10.1016/j.enconman.2010.06.072.
[71] M.M. Heyhat, S. Mousavi, M. Siavashi, Battery thermal management with thermal energy storage composites of PCM, metal foam, fin and nanoparticle, J. Energy Storage 28 (2020) 101235.
[72] A. Wakif, A. Chamkha, T. Thumma, I.L. Animasaun, R. Sehaqui, Thermal radiation and surface roughness effects on the thermo-magneto-hydrodynamic stability of alumina–copper oxide hybrid nanofluids utilizing the generalized Buongiorno's nanofluid model, J. Therm. Anal. Calorim. 143 (2021) 1201–1220.
[73] W. Yu, S.U.S. Choi, The role of interfacial layers in the enhanced thermal conductivity of nanofluids: A renovated Maxwell model, J. Nanopart. Res. 5 (2003) 167–171.
[74] M. Khalili Najafabadi, K. Hriczó, G. Bognár, Entry length correlations for alumina-water nanofluid in laminar pipe flow, Int. J. Therm. Sci. 197 (2024) 108808.
[75] Y. Zhu, H. Chen, J. Zhang, G. Xiao, M. Yi, Z. Chen, C. Xu, Effect of interface layer on the enhancement of thermal conductivity of SiC-Water nanofluids: Molecular dynamics simulation, J. Mol. Graph. Model. 127 (2024) 108696.
[76] J. Chinnam, D.K. Das, R.S. Vajjha, J.R. Satti, Measurements of the surface tension of nanofluids and development of a new correlation, Int. J. Therm. Sci. 98 (2015) 68–80.
[77] A.A. Avramenko, D.G. Blinov, I.V. Shevchuk, Self-similar analysis of fluid flow and heat-mass transfer of nanofluids in boundary layer, Phys. Fluids 23 (8) (2011).

[78] A.A. Avramenko, D.G. Blinov, I.V. Shevchuk, A.V. Kuznetsov, Symmetry analysis and self-similar forms of fluid flow and heat-mass transfer in turbulent boundary layer flow of a nanofluid, Phys. Fluids 24 (9) (2012).
[79] N. Samkhaniani, M.R. Ansari, The evaluation of the diffuse interface method for phase change simulations using OpenFOAM, Heat Transfer - Asian Res. 46 (8) (2017) 1173–1203.
[80] A. Yahyaee, A.S. Bahman, H. Sørensen, A benchmark evaluation of the isoadvection interface description method for thermally–driven phase change simulation, Nanomaterials 12 (10) (2022) 1665.
[81] A. Yahyaee, A.S. Bahman, K. Olesen, H. Sørensen, Level-set interface description approach for thermal phase change of nanofluids, Nanomaterials 12 (13) (2022) 2228.
[82] A. Esmaeeli, G. Tryggvason, Computations of film boiling. Part I: numerical method, Int. J. Heat Mass Transfer 47 (25) (2004) 5451–5461.
[83] P.J. Berenson, Film-boiling heat transfer from a horizontal surface, J. Heat Transf. 83 (3) (1961) 351–356.
[84] A.A. Avramenko, I.V. Shevchuk, N.P. Dmitrenko, A.A. Moskalenko, P.N. Logvinenko, Unsteady convective heat transfer in nanofluids at instantaneous transition to film boiling, Int. J. Therm. Sci. 164 (2021) 106873.